SIMPLIFIED GRINDING MILL CIRCUIT MODELS FOR USE IN PROCESS CONTROL

by

Johan Derik le Roux

Submitted in partial fulfilment of the requirements for the degree

Master of Engineering (Electronic Engineering)

in the

Department of Electrical, Electronic and Computer Engineering
Faculty of Engineering, Built Environment and Information Technology
UNIVERSITY OF PRETORIA

October 2012

SUMMARY

SIMPLIFIED GRINDING MILL CIRCUIT MODELS FOR USE IN PROCESS CONTROL

by

Johan Derik le Roux

Promoters:	Prof I. K. Craig
Department:	Electrical, Electronic and Computer Engineering
University:	University of Pretoria
Degree:	Master of Engineering (Electronic Engineering)
Keywords:	comminution, grinding, milling, modelling, model reduction, run-of-mine ore, simulation

A grinding mill circuit forms a crucial part in the energy-intensive comminution process of extracting valuable metals and minerals from mined ore. The ability to control the grinding mill circuit is of primary importance to achieve the desired product specification with regards to quality and production rate. In order to achieve control objectives an accurate dynamic model of the milling circuit is required. Phenomenological models are preferred over linear-time-invariant models since the latter cannot describe the non-linear behaviour of the process. However, the available phenomenological models of grinding mill circuits are usually complex, use large parameter sets and are mostly aimed towards steady-state design of grinding mill circuits. This study investigates simplified non-linear dynamic models of grinding mill circuits suitable for process controller design.

In the first part of this study, the number of size classes in a cumulative rates model of a grinding mill circuit is reduced to determine the minimum number required to provide a reasonably accurate model of the circuit for process control. Each reduced size class set is used to create a non-linear cumulative rates model which is linearized to design a linear model predictive controller. The accuracy of a model is determined by the ability of the corresponding model predictive controller to control important process variables in the grinding mill circuit as represented by the full non-linear cumulative rates model.

The second part of the study validates a simple and novel non-linear model of a run-of-mine ore

grinding mill circuit developed for process control and estimation purposes. This model is named the *Hulbert*-model and makes use of the minimum number of states and parameters necessary to produce responses that are qualitatively accurate. It consists of separate feeder, mill, sump and hydrocyclone modules that can be connected to model different circuit configurations. The model uses five states: rocks, solids, fines, water and steel balls. Rocks are defined as too large to be discharged from the mill, whereas solids, defined as particles small enough to leave the mill, consist of out-of-specification coarse ore and in-specification fine ore fractions. The model incorporates a unique prediction of the rheology of the slurry within the mill. A new hydrocyclone model is also presented. The *Hulbert*-model parameters are fitted to an existing plant's sampling campaign data and a step-wise procedure is given to fit the model to steady-state data. Simulation test results of the model are compared to sampling campaign data of the same plant at different steady-state conditions.

OPSOMMING

VEREENVOUDIGDE MAALKRINGLOOPMODELLE VIR GEBRUIK IN PROSESBEHEER

deur

Johan Derik le Roux

Promotors:	Prof I. K. Craig
Departement:	Elektriese, Elektroniese en Rekenaar-Ingenieurswese
Universiteit:	Universiteit van Pretoria
Graad:	Magister in Ingenieurswese (Elektroniese Ingenieurswese)
Sleutelwoorde:	komminusie, maling, modelering, modelreduksie, onbehandelde erts, simulasie

'n Maalkringloop vervul 'n kritiese rol in die energie-intensiewe kommunisie proses om waardevolle metale en minerale uit gemynde erts te haal. Die vermoë om die maalkringloop te beheer is van primêre belang om die verlangde produkspesifikasie in terme van kwaliteit en produksietempo te behaal. 'n Akkurate model van die proses word benodig om die beheerdoelwitte te behaal. Fenomenologiese modelle word bo lineêr-tyd-invariante modelle verkies aangesien laasgenoemde nie die nie-lineêre eienskappe van die proses kan beskryf nie. Hoe dit sy, die beskikbare fenomenologiese modelle van maalkringlope is gewoonlik kompleks, maak gebruik van groot parameterstelle en word meestal vir gestadigde-toestand ontwerp van maalkringlope gebruik. Hierdie studie ondersoek vereenvoudigde nie-lineêre dinamiese maalkringloopmodelle wat geskik is vir prosesbeheerder ontwerp.

In die eerste deel van die studie word die aantal erts grootte-klasse van 'n kumulatiewe tempo model van 'n maalkringloop verminder om die minimum aantal grootte-klasse te bepaal wat 'n redelike akkurate model van die maalkringloop vir prosesbeheer gee. Elke verminderde grootte-klas stel definieer 'n nie-lineêre kumulatiewe tempo model wat gelineariseer word om 'n lineêre model voorspellende beheerder te ontwerp. Elke beheerder word gebruik om die maalkringloop soos beskryf deur die nie-lineêre kumulatiewe tempo model te beheer. Die akkuraatheid van 'n model word bepaal deur die vermoë van die ooreenstemmende beheerder om belangrike prosesveranderlikes in die

maalkringloop te beheer.

Die tweede deel van die studie valideer ’n eenvoudige en nuwe nie-lineêre model van ’n onbehandelde erts maalkringloop wat ontwikkel is vir prosesbeheer en afskatting. Die model word die *Hulbert*-model genoem en maak gebruik van die minimum aantal toestandveranderlikes en parameters wat benodig word om kwalitatiewe akkurate reaksies te gee. Die model bestaan uit afsonderlike voerder, meul, dreineerbak en sikloon eenhede wat sodanig gekoppel kan word om verskillende kringbaan konfigurasies te modelleer. Die model maak gebruik van vyf toestandveranderlikes: rotse, soliede en fyn erts, water en staalballe. Rotse word gedefinieer as erts wat te groot is om uit die meul te vloei. Soliede erts is wel klein genoeg om die meul te verlaat en bestaan uit buite-spesifikasie growwe erts en binne-spesifikasie fyn erts. Die model voorspel die reologie van die slyk in die meul op ’n unieke wyse. ’n Nuwe sikloon model word ook voorgehou. ’n Stapsgewyse prosedure word beskryf van hoe die *Hulbert*-model parameters tot bestaande aanlegdata gepas word. Simulasie resultate van die model word vergelyk met aanlegdata van verskeie gestadigde toetstande van die aanleg.

ACKNOWLEDGEMENTS

You never stand alone. You always stand on the shoulders of giants. This dissertation would not have realized if it weren't for a number of giants.

The first of the giants is my supervisor Prof Ian Craig. I am not only grateful for his patient and wise mentorship to guide me on the road to become a quality researcher, but also the life-lessons he imparted.

During the completion of this research I had the privilege of working with Dr Adrian Hinde and Dr Dave Hulbert, who are both giants in the comminution industry in their own right. My knowledge of comminution modelling can be contributed to the generous knowledge and insights they shared.

I would also like to thank my father and mother for granting me the opportunity to study. Who I am today is mostly Gawie and Irene le Roux's fault, and I could not be more grateful. A great deal of thanks is owed to my girlfriend, Madeleine, my two sisters, Liezl and Annine, and my brother in-law, Peter. Through their unrelenting humour, they have contributed greatly to my sanity during the completion of this dissertation.

Lastly, I am eternally grateful for the grace offered to me by The Greatest Giant to complete this work.

LIST OF ABBREVIATIONS

AG	Autogenous
JKMRC	Julius Kruttschnit Mineral Research Centre
MPC	Model Predictive Control
NRMSE	Normalised root mean squared error
PI(D)	Proportional Integral (and Derivative)
ROM	Run-of-mine
SAG	Semi-autogenous

LIST OF FIGURES

LIST OF TABLES

TABLE OF CONTENTS

CHAPTER 1

INTRODUCTION

The word comminution is derived from the Latin word 'comminuere', which means to break or grind into small fragments. The main reasons for comminuting mined ore are to make the ore more workable and to liberate valuable components such as metals and minerals in the ore from gangue (Stanley, 1987). Once mined ore has been broken into a fine product, the metals or minerals in the ore are separated from gangue by means of separation processes such as flotation or leaching. Finally, a recovery process extracts the metals or minerals from the separation process concentrate to produce the final product.

The term comminution in the mineral processing industry encompasses the following unit operations: crushers, tumbling mills, stirred mills and sizing processes. Although sizing processes do not reduce ore in size, they form a crucial part of any comminution circuit. The process of size reduction of mined ore in mills is not only regarded as the most cost-intensive unit process in the mineral processing industry, but also one of the most important for overall plant performance (Wills, 2006; Wei and Craig, 2009a). The correct selection of the operating condition for a grinding mill circuit can significantly improve the economic performance of the process in terms of improved operating costs, increased production capacity and improved downstream process performance as a result of a consistently fine product (Napier-Munn et al., 1999). The optimal operating set-points can be determined based on variables such as the properties and throughput of processed ore, the metal market prices, energy consumption costs or environmental constraints (Hodouin, 2011). The economic benefit achieved by a controller which maintains a grinding mill circuit at the optimal operating condition, can be assessed according to the framework of Bauer and Craig (2008).

This thesis considers simple non-linear dynamic models of a single-stage closed grinding mill circuit

for process controller design. The main objective of the models are to ease process controller design in order to maintain the grinding mill circuit at optimal operation.

1.1 MOTIVATION AND BACKGROUND

Before a controller for a grinding mill circuit is designed, it is necessary to define the control objectives. The control objectives are mostly to improve the quality of the product (by increasing the fineness of the grind or reducing the product size fluctuations), to maximise the throughput, to decrease the power consumption, to reduce the usage of grinding media such as balls and to improve process stability. These objectives are interrelated and necessitates trade-offs to be made (Craig and MacLeod, 1995; Hodouin, 2011).

The challenges when controlling a grinding process are the strong coupling between variables, large time delays, uncontrollable disturbances, the variation of parameters over time, the non-linearities in the process and instrumentation inadequacies (Chen et al., 2008). Also, important physical properties and characteristics of the fresh feed ore and the ground material are often not measurable in real-time. Measurement instruments contend with a very harsh environment and reliability is often an issue. Apart from large measurement noise, on-line measurements of flow-rates, particle size distributions and equipment hold-up can be inaccurate (Hodouin et al., 2001).

In order to develop good control and optimisation strategies to achieve control objectives and overcome control challenges, accurate and physically meaningful mathematical models that describe the steady-state and dynamic behaviour of a grinding mill circuit over the entire non-linear region of operation are essential. Even though purely steady-state models dominate the mineral processing industry at present, dynamic models of grinding mill circuits are expected to become more common in future (Wills, 2006). Because mined ore is a complex system containing intricately mixed minerals with varying properties (size, hardness, mineral content, micro-cracks and surface characteristics distribution), acceptable dynamic models for process control are not readily available (Hodouin et al., 2001).

There are two general approaches to model a ginding mill. A grinding mill can be seen as a transform between the feed and a product size distribution where the aim is to represent the phenomenon of breakage rather than the underlying physical process. Population balance models are the most popular in this class. On the other hand, a fundamental or mechanistic model of a grinding mill is based on the

interactions of ore particles and elements within the machine on the basis of Newtonian mechanics (Napier-Munn et al., 1999).

The mathematical models that have been most useful for automatic control so far were developed "on-line" by empirical means. Empirically derived linear-time-invariant transfer function models have been successfully used in model based controller strategies (Chen et al., 2007, 2008; Craig and MacLeod, 1996). However, these linear models are restricted to the domain around the nominal operating conditions of the plant and require constant adaptation to changing process operation and ore properties (Hodouin et al., 2001). An emerging control technique for grinding mills is the on-line use of phenomenological models which are a combination of mechanistic and empirical models (Hodouin et al., 2001).

According to Powell and Morrison (2007), future grinding mill models will change from empirical models to mechanistically based models where mineralogical liberation forms an integral part of the models. The aim is to separate ore and machine properties by modelling breakage in terms of the ore interactions within the mill rather than modelling breakage by the mill output (Gupta and Yan, 2006; Napier-Munn et al., 1999; King, 2001).

Detailed fundamental or population balance models of grinding mills are usually thought to be best or necessary to represent the "state of the art". However, they have two potentially serious weaknesses. Firstly, large parameter sets cannot be reasonably fitted accurately from accessible real plant data. Heavy emphasis is placed on non-linear regression techniques and back-calculation to determine the parameters, in which case small measurement errors can lead to large variances in parameter values (Hinde and Kalala, 2009; Powell and Morrison, 2007). Secondly, the detailed models can have internal approximations that transmit and amplify inaccuracies in an unknown way. Generally, detailed models are not invertible in such a way that their parameters and confidence limits can be calculated from data. Because there are so many parameters, a good fit can be obtained by fixing certain parts of the model through wrong adjustments elsewhere.

Apart from the large parameter sets that are difficult to estimate, detailed fundamental or population balance models are usually either too complex or too extensive to use in process controller design. In many cases, these models are developed with steady-state process design rather than dynamic process control in mind. An adaptation of Occam's razor is applied in this dissertation to develop accurate and dynamic models useful for process control: the simpler theory between two competing theories

is preferred if they make the same prediction.

1.2 CONTRIBUTION

This work contributes to the development of two simple grinding mill circuit models that are suitable for process controller design. The following is a list of dissertation contributions:

- A detailed mill model description as defined by the cumulative rates model is presented.
- Two different procedures to reduce the number of ore size classes used by the cumulative rates model are investigated.
- The modelling accuracy of the cumulative rates model with reduced size class sets is investigated.
- The ability of a controller based on a reduced size class set to control a grinding mill circuit is investigated.
- A detailed description of a simple and novel model, called the *Hulbert*-model, is presented.
- A step-wise procedure is described to fit the *Hulbert*-model parameters to steady-state sampling campaign data.
- The *Hulbert*-model is validated with actual sampling campaign data.

1.3 PUBLICATIONS

The following publications have resulted from this work:

- Le Roux, J.D., Craig, I.K., Hulbert, D.G., Hinde, A.H., April 2012., Analysis and validation of a run-of-mine ore grinding mill circuit model for process control, In: Proc. 8th Int. Comminution Symp., Cape Town, South Africa.
- Le Roux, J.D., Craig, I.K., Hulbert, D.G., Hinde, A.H., 2012., Analysis and validation of a run-of-mine ore grinding mill circuit model for process control, Minerals Eng., Articles in Press.

- Le Roux, J.D., Craig, I.K., Sept. 2012., Size class reduction in a cumulative rates model for a grinding mill circuit. In: Proc. IFAC Workshop Automation Mining Mineral Metal Industries, Gifu, Japan.

- Le Roux, J.D., Craig, I.K., 2012., Reducing the number of size classes in a cumulative rates model used for process control of a grinding mill circuit, Powder Technology, Submitted for Review.

1.4 ORGANISATION

The dissertation is organised in the following manner. Chapter 2 provides a detailed description of grinding mill circuits as well as background with regards to population balance models. In chapter 3 the number of size classes that define an accurate model of the circuit for process control is investigated. Chapter 4 describes the simple and novel *Hulbert*-model of the grinding mill circuit developed for process control and estimation purposes. The *Hulbert*-model is also fitted to steady-state sampling campaign data and validated in chapter 4. Concluding remarks and suggestions for further research are given in chapter 5.

CHAPTER 2

THEORY OF MILLING

2.1 INTRODUCTION

This chapter aims to provide a description of the milling process, the different units in the grinding mill circuit and a brief background on population balance modelling of grinding mills.

2.2 PROCESS DESCRIPTION

The single stage closed-circuit milling process considered in this dissertation is illustrated in Fig. 2.1. The three main units in this figure are the grinding mill, the sump and the hydrocyclone. The mill receives four streams: mined ore, water, steel balls to assist with the breakage of ore and underflow from the hydrocyclone. Thus, the total mill load or charge consists of water, ore and steel balls. As the mill rotates, the ore in the mill is broken into fine particles by the steel balls and the ore itself. In this manner the valuable mineral or metal is liberated from the gangue. The ore in the mill mixes with the water to create a slurry. The slurry in the mill is then discharged to a sump. The slurry from the mill can be discharged either by overflow or through a discharge screen. In the case of the screen, the particle size of the discharged slurry from the mill is limited by the aperture size of the screen. The slurry in the sump is diluted with water before it is passed via a pump to the cyclone for classification. The hydrocyclone is responsible for the separation of the in-specification material and out-of-specification material in the slurry discharged from the sump. The lighter, smaller and in-specification particles in the slurry pass to the overflow of the hydrocyclone, while the heavier, larger and out-of-specification particles pass to the underflow. The underflow is fed back to the mill to regrind the out-of-specification particles. The overflow is the product of the circuit that is passed to a downstream process. The aim of the circuit is to produce an overflow where a percentage of

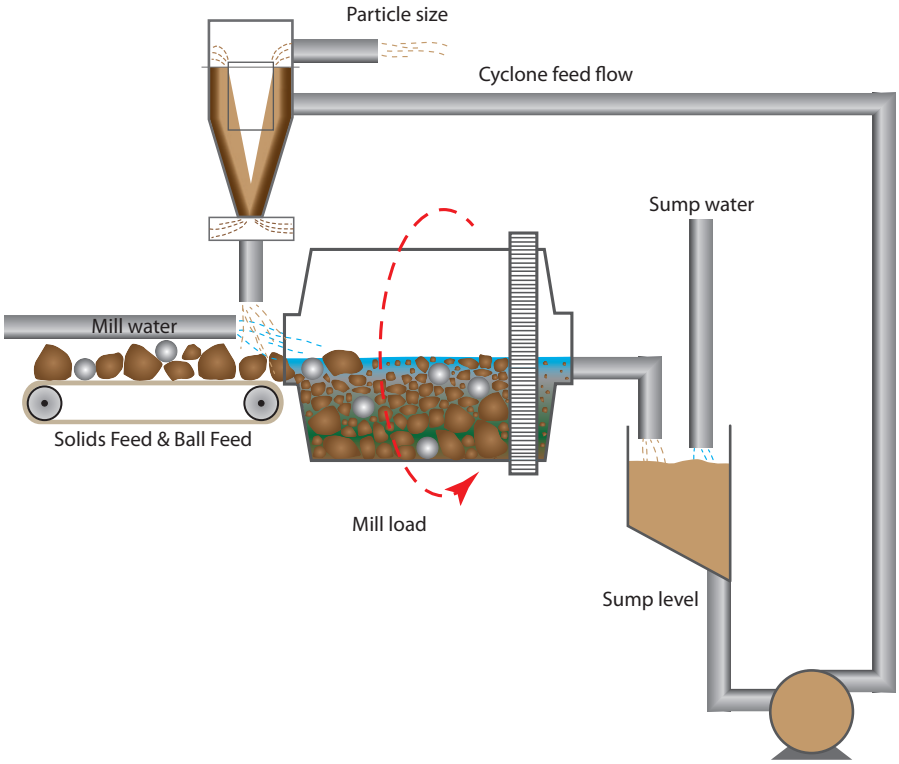

Figure 2.1: A single-stage closed circuit grinding mill.

the particles in the overflow is smaller than the specification size (Stanley, 1987; Coetzee et al., 2010).

The three variables most often controlled in grinding mill circuits are the product particle size, the slurry level in the sump and the cyclone feed density. Because the slurry level in the sump is open-loop unstable, control of this variable is to be expected. But the load within the mill is also open-loop unstable if the discharge from the mill is restricted, which is usually the case, and requires some form of control. Although plants do control this variable, it is controlled less often than the product particle size, slurry level and cyclone feed density. Since throughput and product particle size are dependent on each another, plants that control throughput do this at the expense of product particle size control. The four variables most commonly manipulated on grinding mill circuits are the flow-rate of water to the mill and to the sump, the flow-rate of slurry to the cyclone, and the feed-rate of ore to the mill (Wei and Craig, 2009b).

2.2.1 Grinding mills

The first and most important unit in Fig. 2.1 is the grinding mill. Grinding mills are generally divided into two types: tumbling and stirred mills. A tumbling mill comprises of a large cylinder that is rotated about its horizontal longitudinal axis by an electric motor and imparts motion to the charge via the mill shell. The mill shell is lined with a wear resistant material, called a liner, to protect the shell from being worn away by ball and rock impacts. Raised sections or lifters inside the tumbling mill provide lift to the charge as the mill rotates. Without lifters the charge is lifted very little and the liner is worn away quickly. The grinding medium used to break the ore may be steel rods, balls or the mined ore itself. A stirred mill is a stationary vertical or horizontal tubular shell that imparts motion to the charge by the movement of an internal stirrer (Napier-Munn et al., 1999). This study only considers tumbling mills, which can be divided into four general groups:

- **Autogenous (AG) mills**, where autogenous means self-generating, use only the ore in the mill as grinding media. AG milling can be divided into two groups: run-of-mine (ROM) ore milling and pebble milling. The first type receives ROM ore directly and uses this as grinding media. This type of milling is only suitable for primary grinding. For pebble milling, hard rocks within a certain size class are extracted from the ore feed and used as grinding media. Pebble milling is suitable for any stage of grinding.

- **Semi-autogenous (SAG) mills** are similar to AG mills, but use steel balls and ore as grinding media. Since the power draw of a mill is a function of the bulk density of the load, AG mills draw less power and have a lower grinding capacity than similarly-sized ball and rod mills. To achieve a similar grinding capacity, steel balls are added to an otherwise ROM or pebble AG mill to increase the bulk density of the charge. Usually the volume of steel balls in the total charge volume does not exceed 10%. A SAG mill may also be viewed as a special case of a ball mill (Stanley, 1987). SAG milling is commonly used for primary grinding. The reasons are low operating cost, the increasing need to process large amounts of low-grade ore, their ability to process crushed ore and their reduced grinding media consumption (Salazar et al., 2009).

- **Ball mills** remain the most common mill type for size reduction of ore (Wei and Craig, 2009b). The grinding media for ball mills are steel balls that vary in size from 50 mm to 100 mm in diameter. The mass of balls in the mill accounts for almost 80-85% of the total charge mass and dominates the grinding performance and power draw of the mill. The power draw remains

fairly constant and reduces gradually with the consumption of balls (Napier-Munn et al., 1999). These mills are mainly applied in the first stage of grinding if insufficient pebbles are available in the crushed ore feed to support AG milling (Stanley, 1987).

- **Rod mills** use steel rods as grinding medium that are 100 mm in diameter and 100 mm shorter than the length of the mill. Rod mills can handle coarser ore than other mill types and produce finer particles than crushing. Rod mills are not suitable for closed circuit operation since a concentration of fine ore in the mill feed inhibits the breakage of coarser ore. Since rod mills are essentially fine crushers, they should not be used to produce a final product. Rather, they can be used to feed conventional milling stages (Stanley, 1987). Rod mills are used much less often in the mineral processing industry than the other types of mills.

2.2.1.1 Motion of charge in the mill

The charge of a stationary mill consists of a mixture of grinding media and slurry, occupies less than half the mill volume and lies in the bottom of the mill. As soon as the mill starts to rotate, the charge in the mill is carried up the rising side of the mill to a height that depends on the rotation speed, the shape of the mill lifter and the degree of slip between the mill charge and mill shell.

If the height of lift imparted to the charge is small, the charge at the top of their travel will curve and slide down the rising portion of the charge to the bottom of the mill where it rejoins the rising charge. This is called ‘cascading’.

If the mill speed increases, particles at the top of the rising charge are projected airborne into parabolic paths in which they continue to rise for a short distance before falling back to the bottom of the load. This is called ‘cataracting’. The uppermost point where the charge leaves the mill shell is defined as the ‘shoulder’. The highest vertical point of the airborne particles is defined as the ‘head’. The area where the airborne particles make contact with the mill is defined as the ‘impact toe’ (Stanley, 1987; Coetzee, 2009).

If the mill speed is increased further, centrifugal forces acting on charge particles will be greater than the centripetal component of the weights of the particles. Thus, the mill charge remains in contact with the shell throughout the rotation of the mill. This is called ‘centrifuging’ and occurs at the critical speed of the mill (Stanley, 1987).

Because the circumference of the mill is longer than the path of grinding media, the charge in the mill rotates faster than the mill itself.

It is generally regarded that there are three causes of particle breakage in tumbling mills (Napier-Munn et al., 1999; Stanley, 1987):

- **Impact breakage** occurs when two bodies approach each other with paths of motion perpendicular to the plane of contact. The degree of breakage is directly related to the energy per unit mass that the target particle receives. This type of breakage occurs mainly at the toe of the charge.

- **Abrasion** is a surface phenomenon and occurs when two particles slide over each other under pressure. Small pieces are torn out of the surface of the particles, leaving the parent particles largely intact. This is mostly confined to the area of contact between the rising and descending layers of the charge.

- **Attrition** occurs when a small particle is trapped between to larger particles in conditions similar to abrasion. The small particle is broken in preference to the larger particles. This type of breakage occurs in the same area as abrasion.

Slurry can be discharged from a mill by means of a screen or overflow. AG and SAG mills make use of a rubber or steel screen to keep grinding media inside the mill, while allowing small enough particles in the slurry to flow through the screen and out of the mill. The screen apertures can be round, square or slotted, with reverse taper to keep near-size material from becoming lodged in the apertures. The screen is usually placed parallel to the end of the mill which can either be closed with a discharge trunnion or left completely open. For the slurry to exit via the discharge trunnion, pan-lifters that rotate with the mill direct the slurry that passed through the screen to the discharge trunnion. If the end of the mill is kept open, the slurry flows through the screen and out of the mill by means of gravity. For overflow discharge no screen is placed at the mill end. The mill has an exit hole at the discharge trunnion which is larger than the inlet and the hydraulic gradient between the inlet and outlet drives the slurry through the mill. Ball mills make use of either the overflow or the screen discharge mechanism (Napier-Munn et al., 1999).

2.2.1.2 Operation considerations

The equilibrium of a grinding mill is perturbed when the rate, size distribution or hardness of the ore that is fed to the mill varies. The effect of these variations on the behaviour of the grinding mill will require time to decay. Although it is desirable to control all three variables, usually only feed-rate of ore to the mill can be controlled. A grinding mill circuit has to contend with feed ore hardness and size distribution variations as disturbances (Napier-Munn et al., 1999). However, a manner of feed size distribution control is possible if ROM ore is not used. In Steyn (2011) the ore fed to the mill is a controlled ratio of ore from a coarse ore silo and ore from a fine ore silo.

Changes in the feed-rate of ore and feed ore hardness does not directly change the power draw. The feed-rate and feed hardness change the charge volume and consequently the power draw changes in accordance with the change in charge volume. Changes in the feed size distribution will result in changes in the grinding media size distribution, which will affect the breakage characteristics in the mill (Napier-Munn et al., 1999).

AG and SAG mills respond differently to feed size distribution variations. For AG mills the size distribution of the ore should provide large enough rocks to generate sufficient kinetic energy to break smaller rocks. Also, a sufficient amount of large rocks should be available to maintain a high frequency of breakage collisions. A balance between the number of rocks and the feed size distribution must be maintained to achieve optimum performance. AG mills usually perform best with coarser ore feeds (Napier-Munn et al., 1999). In SAG mills, as the volume of balls increase, the coarse feed rocks will contribute less to the overall grinding media. Instead, the rocks become a burden that requires grinding. If the size of the feed is reduced, the grinding burden will be lessened and the mill performance will improve. This is also the case for ball mills where a reduction in feed size results in an increase in throughput (Napier-Munn et al., 1999).

Because hard ore will often produce a coarser feed size to the mill, it is difficult to separate the effect of feed size distribution and feed ore hardness on milling performance. Also, AG and SAG mills respond differently to changes in feed ore hardness. Soft ore results in an increased throughput in SAG mills since coarse ore is broken more easily by the steel balls. Yet, the product size usually becomes coarser because the coarse ore spends less time in the mill being worn away by abrasion. In contrast to SAG mills, AG mills rely exclusively on the feed ore for their grinding media. Soft ore will break more readily than hard ore and will generate less quantities of larger grinding media.

However, if the ore is too hard, the large rock grinding media may not have sufficient energy to break the ore into fine sizes. For both too soft ore and too hard ore, the throughput of an AG mill will be limited (Napier-Munn et al., 1999).

AG milling produces a fine grind at a fairly low throughput and SAG milling produces a coarse grind at a fairly high throughput. The introduction of balls to the mill increases impact breakage and causes coarse ore to be broken down much more rapidly than by the slower abrasion process. However, the rapid rate of coarse ore breakage by steel balls reduces the availability of rock grinding media responsible for producing finer particles in the product and reduces the time that coarse ore is worn away by means of abrasion to produce a finer product. If the ball charge volume is increased to very high levels of more than 15%, the large number of balls compensate for the loss of rock grinding media and the effect on the product size distribution is reduced (Napier-Munn et al., 1999).

By running a mill in closed circuit with a fine classifier such as a hydrocyclone, a finer product can be obtained. If the interstices between the grinding media in a mill are filled with slurry, attrition breakage of the smaller particles in the slurry is promoted. If a mill is run in closed circuit with a fine classifier such as a hydrocyclone, the underflow from the classifier recycles slurry back to the mill. If the flow of recycle slurry is not too great, slurry will accumulate in the grinding media interstices. This promotes attrition breakage which will produce a finer product out of the mill. If the recycle of slurry is too much, a slurry pool will build up at the toe of the charge. Since grinding media needs to penetrate the slurry pool, the kinetic energy available for impact breakage is reduced. Thus, the power draw of the mill reduces along with the rate at which coarse ore is reduced in size when a slurry pool forms at the toe of the charge (Napier-Munn et al., 1999).

2.2.1.3 Optimization considerations

Optimization criteria of a grinding mill circuit depend on the process requirements and plant economics. The typical criteria are listed below (Napier-Munn et al., 1999):

- **Throughput** of a mill is limited by the charge volume, power availability and mill speed. The throughput can be increased by increasing the charge volume in the mill until the mill contents start to spill. Since an increase in the charge volume results in increased power draw, it is necessary to ensure that the maximum power of the mill motor is not exceeded. A higher throughput is also obtained if the rotating speed of the mill is increased.

- **Grind size** is predominantly a function of the ore in open-circuit AG/SAG mills. Modest manipulations of the grind size can be made by changing the mill speed, ball load and ball size. The grind size in a closed-circuit AG/SAG mill can be manipulated by changing the classifier performance. For optimal throughput, the classifier should not return particles that fall within the correct size class.

- **Specific power consumption** (kWh/t) gives an indication of the efficiency of the mill. A higher ball load and charge volume generally reduces the specific power consumption.

- **Steel consumption** depends on the ore, liner and ball material. Low charge levels in SAG mills cause balls to collide with exposed liners and lifters. High ball levels also increase the consumption of steel. The ball level should thus be kept at the minimum allowable level to maintain throughput demands.

2.2.2 Sump

The slurry discharged from the mill flows into the sump, which can be considered as an ideal mixer. The sump is the second unit in Fig. 2.1. The pump at the discharge of the sump is responsible for pumping the slurry in the sump to the hydrocyclone. Large changes in the sump level can lead to the generation of large disturbances. For high slurry levels the mixing of slurry deteriorates and stagnant zones are created within the sump. The sloughing of solids at high sump levels can result in erratic discharge. For low slurry levels air is entrained and pump capacity is lost. The sump level will increase until the air entrainment is resolved. Because the slurry levels for the initiation and termination of air entrainment is different, limit cycle oscillations can be generated (Hinde and King, 1978).

The flow-rate of the slurry from the pump is not only a function of the pump impeller speed, but also of the total dynamic head. The relationship between the dynamic head and the slurry flow-rate influences the effectiveness of different control strategies. The sump level can be controlled by means of water addition, a variable speed pump motor or recycle of classified slurry back to the sump. Because the dynamic head and the slurry flow-rate will change when the slurry level or slurry density changes, sump level control by water addition often leads to undesirable oscillatory behaviour and amplification of process disturbances (Hinde and King, 1978).

2.2.3 Hydrocyclone

The slurry pumped from the sump in Fig. 2.1 enters the hydrocyclone tangentially and is constrained to move in a circular path. Each particle in the slurry experiences a centrifugal force acting outwards, a displacement force acting inwards and the drag force acting inwards. Therefore: nett centrifugal force = centrifugal force - displacement force - drag force. As the radius of a particle decreases, the nett centrifugal force decreases. Thus, separation according to size occurs with larger particle tending to displace smaller particles away from the hydrocyclone walls. For a particle that is sufficiently small the drag force will exceed the centrifugal force and the particle will move to the centre of the cyclone. Thus, the coarser particles move to the hydrocyclone walls where they join the downward flow spiral which exits at the apex of the hydrocyclone. The fine particles and the majority of the water move to the center of the hydrocyclone to join the upward flow spiral which exits via the vortex finder (Stanley, 1987; Napier-Munn et al., 1999).

Therefore, a hydrocyclone separates the feed slurry into material coarser and finer than a specific size. The separation size is called the cut-size or the classification size and is chosen according to the process requirements. The coarse material joins the underflow and returns to the mill for further grinding. The fine material joins the overflow and is passed to the next process stage, which can either be another size reduction process or a beneficiation stage such as flotation, leaching or gravity concentration (Napier-Munn et al., 1999).

The objective for hydrocyclone operation is to achieve the sharpest possible separation at the correct classification-size with the optimal division of water between the overflow and underflow. The main variables available to optimize the cyclone performance are the cyclone geometry and the feed conditions (Napier-Munn et al., 1999). A real cyclone cannot achieve a sharp cut for the following reasons (Stanley, 1987; Napier-Munn et al., 1999):

- There is turbulent mixing in the cyclone.
- Coarse material leaks across the top of the cyclone to the overflow.
- Fines trapped between coarser particles at the cyclone wall report to the underflow.
- The particle shape, size and density play a significant role in hydrodynamic classification.

The major problem in hydrocyclone control is that maximum system production is achieved at the constraint imposed by the apex capacity of the cyclone, i.e. the optimal conditions correspond to high underflow volume throughput at low water content. This means that small perturbations can cause erratic behaviour and roped slurry discharge from the cyclone underflow (Hinde and King, 1978).

2.3 CONTROL OF GRINDING MILL CIRCUITS

Even though process control can be considered as a mature technology for a mature industry with benefit to the operating and economic performance of a process, three main problems face the mining, mineral and metal processing industry in terms of process control: the design of accurate process models, development of advanced process control strategies and realistic approaches to system analysis and synthesis for complex systems (Dochain et al., 2008). Poor measurement systems and inaccurate modelling of industrial processes contribute to the inability of current control technology to provide satisfactory results. For example, state variable observer design based on data reconciliation techniques with mass and energy conservation models struggles in real-time environments because the models do not take process dynamics into account. To overcome the challenges that face control in the process industry, one avenue is further research to generate accurate process models at low cost. A method to develop proper low-cost process models, which remains a significant challenge for complex processes, could expand opportunities for new advanced process controller applications (Craig et al., 2011).

To illustrate the different approaches available to control grinding mill circuits, Pomerleau et al. (2000) compare the performance of various control algorithms in simulation for a grinding mill circuit. It was found that Proportional Integral and Derivative (PID) controllers perform as well as model-based controllers if the time delays are much smaller than the dominant time constants, predictive and algebraic controllers perform equally well in stochastic environments if no noise model is available, and adaptive controllers perform better than fixed controllers for parametric disturbances or non-linearities. According to the survey of Wei and Craig (2009b), the application of advanced process controllers in industrial grinding mill circuits is much less than the application of the most prevalent control technology in use, PID control. This observation supports the survey results of Qin and Badgwell (2003) which shows that the application of advanced process control technology, specifically model predictive control, is not yet common practice in the mining and metallurgy industry.

However, there have been numerous documented applications of advanced process control on pilot plants and industrial grinding mill circuits indicating the advantages of advanced process control. Hulbert (1983) used Inverse Nyquist array techniques to design a multivariable controller for a pilot grinding mill circuit. Craig and MacLeod (1996) successfully implemented a μ-controller on an industrial circuit. More recently, Chen et al. (2007) and Chen et al. (2008) illustrated the application of model predictive control to industrial grinding mill circuits. The models used in the design of these advanced process controllers were linear time-invariant transfer function models.

An essential feature of model-based controller design is the availability of mathematical models that accurately describe the steady-state and dynamic characteristics of the grinding mill process (Hodouin et al., 2001). The disadvantage of linear time-invariant transfer function models are that they remain limited to the operating region of the grinding mill circuit during the derivation of the transfer functions. The non-linear behaviour of the grinding mill circuit over a large operating region is not easily modelled by the linear transfer function models.

There are a number of nonlinear dynamic models available for grinding mill circuits. These models can be divided into fundamental models and population balance models. Fundamental models consider the direct interaction between ore particles and elements within the mill mostly based on Newtonian mechanics. These models provide valuable insight into the behaviour of mill charge. An example is the simulation of tumbling mills using discrete element modelling to capture the behaviour of charge in mills and predict individual particle trajectories, power draw and distribution of contact forces and energies between collisions. An overview of the techniques underlying the application of discrete element modelling to grinding mill circuits can be found in Mishra (2003a,b). Fundamental models can also be used to describe cyclones, as seen in Narasimha et al. (2012). Because the models considered in this thesis are population balance models which model the circuit as a transform between the feed and discharge, fundamental models were not investigated in this dissertation. Also, fundamental models are computationally expensive and not easily used in real-time control simulations.

Although population balance modelling is discussed in the following section, two of the few dynamic population balance models for SAG and AG mills available in literature are mentioned here. Valery Jr. and Morrell (1995) presents a conceptual dynamic SAG and AG population balance model developed at the Julius Kruttschnit Mineral Research Centre (JKMRC). Although this model was not simulated and compared with dynamic plant data, the model is used by Apelt and Thornhill (2009) for inferential

measurement of SAG mill parameters. Apelt and Thornhill (2009) performed a validation study of the inferential measurement models against dynamic plant data. The inferential measurement models showed various limitations, especially with regards to mill charge fraction estimates. From the study it is difficult to ascertain the accuracy of the model by Valery Jr. and Morrell (1995) to simulate the dynamic behaviour of a mill. Even so, the steady-state form of this model can be considered as the standard approach to modelling grinding mill circuits.

A dynamic population balance model for SAG grinding mills are found in both Amestica et al. (1996) and Salazar et al. (2009). Both models make use of a cumulative breakage rate to describe the breakage of ore inside the mill. The latter of the two models was validated with dynamic plant data and responded adequately from a qualitative viewpoint to changes in input variables. However, the model required continuous re-calibrations in order to adapt to new conditions.

2.4 POPULATION BALANCE MODELS OF GRINDING MILLS

The modelling and simulation of grinding mills is an indispensable step in the design of a circuit for specific applications (Morrell, 2004; Amestica et al., 1996). The simulation environment can simulate entire comminution circuits and evaluate the designs according to a variety of criteria, e.g. throughput, power draw and product size (Morrell, 2004). The success of the simulation is dependent on the type and accuracy of the models used. A dynamic model needs to be at least qualitatively accurate (i.e. the rate and direction of changes in input, output an internal variables are accurate) if the model is used for the design of control systems or estimating mill variables. A model that is also quantitatively accurate provides a simpler transition between results from simulation to the actual plant (Amestica et al., 1996).

The frequency of breakage events in a mill is related to the total mass of grinding media and the rate at which the mill rotates. The energy associated with particle breakage is related to the mass of the target rocks and the energy of the grinding media. The minimum required knowledge for a model of a milling circuit is the (Morrell, 2004):

- frequency of breakage events for each size fraction;
- energy associated with each breakage event;
- size distribution of products from each breakage event; and

- transport of slurry through end discharge grates.

The processes above are related to the size reduction, throughput and power response of the mill, which can be predicted simultaneously from one overall model if the model is configured correctly (Morrell, 2004).

A useful framework to encompass the size reduction process in the comminution process is a population balance model, of which the perfectly mixed ball mill model of Whiten (1974) is a good example. Assuming a perfectly mixed mill removes any mixing complications and makes the model practically useful (Napier-Munn et al., 1999). An assumption for population balance models is that the production of ground material per unit time is only a function of the mass of the size fraction within the mill, i.e. a rate constant exists which describes the rate of disappearance. Although this assumption simplifies the model, it is not justifiable over a wide range of operation. If the operating conditions on an industrial circuit remain fairly constant, these models are useful and efficient in plant control (Napier-Munn et al., 1999). The basic structure of any population balance model is described by the equation below.

$$Accumulation = Inflow - Outflow + Generation - Consumption \tag{2.1}$$

Population balance models have the capacity to represent the steady-state and dynamic performance of a grinding mill. Yet, it should be remembered that a population balance model of a grinding mill is not a model which describes the breakage process inside the mill itself. Rather, it is a framework which maintains mass integrity and describes the output of equipment (Morrell, 2004; Powell and Morrison, 2007). It represents the phenomenon of breakage instead of the underlying physical or mechanistic principles (Napier-Munn et al., 1999).

Only three functions are required for a population balance model to describe the behaviour of the size distribution and composition of material inside a mill, the selection, appearance and discharge functions. The selection function is the proportion of a specific material selected for breakage per unit of residence time. The appearance function is sometimes called the breakage function and is the degree to which the selected particle type undergoes breakage. The appearance function can also be described as the size distribution of a particle once it has been broken. The product of the selection and appearance function is called the breakage rate. Lastly, the discharge function describes the selection of particles which are to be removed from the mill (Powell and Morrison, 2007; Hinde and Kalala, 2009).

The particle size distribution of material flow throughout the mill circuit can be determined by sieving samples of streams on a series of sieves of decreasing aperture size. It is common for the sieve aperture sizes to reduce by a factor of $2^{0.5}$. The percentage of the total sample mass retained on the sieve and the percentage of material that passes through the sieve can be reported in two ways. A differential distribution gives the percentage of the total sample mass retained between two successive sieves, whereas a cumulative distribution gives the combined mass percentage either coarser or finer than each sieve (Stanley, 1987). The sizes are given by x_i, where the subscript i serves as an index to reference each size class.

The size-by-size (differential distribution) solids mass balance and a water balance model developed by the JKMRC is shown below (Morrell, 2004; Apelt et al., 2002). It treats the mill as perfectly mixed. The solids mass balance model is:

$$\frac{\partial s_i}{\partial t} = f_i - d_0 c_i s_i + \sum_{j=1}^{i-1} r_j s_j a_{ij} - (1 - a_{ii})\, r_i s_i \tag{2.2}$$

where f_i is the mill feedrate of solids in size class i (t/h), r_i is the breakage rate for particles of size class i and varies with operating conditions within the mill (h^{-1}), a_{ij} is the appearance function, s_i is the mill rock charge in size i (t), c_i is the discharge grate classification function value for size class i (probability of particle passing through discharge grate) and d_0 is the maximum mill discharge rate constant (h^{-1}).

The water balance model is:

$$\frac{\partial s_w}{\partial t} = f_w - d_0 s_w \tag{2.3}$$

where f_w is the mill water feedrate (t/h), s_w is the mill water charge (t) and d_0 is the same as for the solids mass balance model.

The simplicity of the model give rise to both strengths and weaknesses. It is easy to use and very versatile, but it lacks the physical description of the sub-processes on which size reduction depends. For this reason, supplementary models for the appearance function a_{ij}, breakage rate r_i and power draw of the mill are defined to make the model useful (Morrell, 2004). Because the JKMRC model treats breakage as a statistical average of discrete single-particle impact events, it is possible for some particles to remain unbroken after a low-energy event so that values of a_{ii}, in eq. (2.2) do not necessarily have zero values.

A difficulty in applying this model is the determination of the appearance function and the subsequent

breakage rate for the ore under investigation. The major issue is that the breakage rates are dependent on both the machine and the ore, are a function of interdependent variables, and can be more dependent on the modelling technique than be a true estimate of the rates of breakage in the device. According to Powell and Morrison (2007), the modelled breakage rate has no physical significance since it is merely a construct of the model structure and the assumptions regarding selection and discharge functions. Thus, the breakage rate absorbs any unknowns and inaccuracies of the model. It is only by means of exhaustive laboratory test work and simplifying assumptions that the function parameters can be estimated (Powell and Morrison, 2007). Because of the heavy reliance on back-calculation to determine parameters, small measurement errors can often lead to large variances (Hinde and Kalala, 2009).

2.5 CONCLUSION

This chapter presented a description of the operation of the three main units - the mill, the sump and the hydrocyclone - in the grinding mill circuit shown in Fig. 2.1. The widely accepted JKMRC population balance model of the grinding mill has also been discussed.

CHAPTER 3

SIZE CLASS SET REDUCTION FOR A CUMULATIVE RATES MODEL

3.1 INTRODUCTION

When modelling a grinding mill circuit with a population balance model, the question arises how many and which size classes should be used to characterize the material in the circuit. The models in the studies of Amestica et al. (1996) and Apelt et al. (2002) use 27 size classes, the model of le Roux et al. (2012) uses only 3 size classes and the model of Bascur and Herbst (1985) uses only 2 size classes to characterize ore. The latter two models were developed for process control purposes and the model in le Roux et al. (2012) has been used in a robust nonlinear model predictive controller for a grinding mill circuit (Coetzee et al., 2010). The advantage of a model with fewer size classes is that it is simpler to incorporate in a model-based controller scheme. However, a model-based controller is dependent on an accurate and reliable process model. Therefore, it is of interest to determine the minimum number of size classes that yields a good model for process control purposes.

It can be argued that a model should have a minimum of four or five size classes. The size classes should account for the usually bimodal size distributions of ore feed, mill discharge and hold-up. The size classes should therefore reflect the following:

- Slimes from zero to a few microns that have transport behaviour that follows that of water. (The JKMRC model (Apelt et al., 2002) assumes that the specific discharge rate function is constant up to about 1 mm.)

- Fines from a few microns to around 13-25 mm that should obey normal breakage behaviour

and would be the typical feed for a conventional ball mill.

- Critical size material from 13-25mm to 50-100mm that exhibits abnormal breakage behaviour. This material does not self-break, is difficult to grind and is inefficiently broken by coarse rock and steel grinding media. This is particularly true for AG and SAG mills.

- Rocks coarser than about 100 mm that self-breaks to form pebble grinding media, but leads to critical size problems.

This chapter investigates how many size classes are necessary to accurately simulate a grinding mill circuit with a cumulative rates model for process control purposes. A base set of 25 size classes is reduced to smaller sets and each reduced set is used to model the circuit. Since the cumulative rates model is non-linear, each model is linearized before it is used to design a linear model-based controller. The controllers are implemented on a grinding mill circuit simulated by the non-linear model with 25 size classes. The controller performance is used as a measure of the accuracy with which a size class set models the circuit. Because the controllers are model-based, the performance also indicates the least number of size classes that should be included in a model for process control (le Roux and Craig, 2012).

3.2 A SIMPLIFIED MODEL: THE CUMULATIVE RATES MODEL

The cumulative rates model in Hinde and Kalala (2009) is a simplified population balance model based on the assumption that only one function is necessary to describe grinding kinetics inside the mill, as illustrated in Bascur and Herbst (1985); Laplante et al. (1987). This function is the cumulative breakage rate function, which is defined as the rate per unit mass that a given species coarser than a given size breaks to below that size (Austin et al., 1993; Amestica et al., 1993, 1996; Salazar et al., 2009). This assumption gives an advantage over the population balance model of Whiten (1974) and the popular JKMRC model described in Apelt et al. (2002) which require two functions, the breakage rate and the appearance function, to describe the grinding kinetics. The parameters of the breakage function in the cumulative breakage rate model can be determined uniquely from direct plant measurements (Hinde and Kalala, 2009). In comparison, the breakage rate and appearance function parameters for the population balance model of Apelt et al. (2002) need to be determined by back-calculation or non-linear regression techniques (Coetzee, 2009; Hinde and Kalala, 2009).

A drawback in the cumulative breakage rate model is the assumption that the cumulative rates of breakage of ore above a given size x_i is unaffected by the grinding environment and the structure of the size distribution above x_i. This drawback also holds for the parameters of the breakage rate and appearance function of the models of Whiten (1974) and Apelt et al. (2002). If grinding conditions depart significantly from those used to derive the cumulative breakage rate parameters, it is possible to get negative flow rates in some of the size classes - especially the smaller size classes. This implies that the parameters need to be adjusted according to the changes in the grinding conditions. Including the effect of grinding environment changes on the cumulative breakage rate function is a possible improvement for the model, but does not form part of this study. It can be assumed that for a SAG mill the values for the cumulative breakage rate function remain fairly constant as long as the ball filling and internal charge level remain fairly constant (Amestica et al., 1993).

3.3 THE CUMULATIVE RATES MODEL DESCRIPTION

A SAG mill with an end-discharge grate in a single-stage closed circuit configuration, as shown in Fig. 3.1, is considered in this chapter. The manipulated and controlled variables in Fig. 3.1 are described in Table 3.1. A complete process description can be found in Chapter 2.

The cumulative rates model of Hinde and Kalala (2009), as it defines the mill, the sump and the hydrocyclone in Fig. 3.1, is described here. The nomenclature of the model can be seen in Tables 3.2 and 3.3.

Table 3.1: Description of circuit variables

Variable	Description
	Manipulated Variables
CFF	flow-rate of slurry to the cyclone [m^3/h]
MFS	feed-rate of ore to the mill [t/h]
MIW	flow-rate of water to the mill [m^3/h]
SFW	flow-rate of water to the sump [m^3/h]
	Controlled Variables
PSE	product particle size estimate [%]
JT	fractional volumetric filling for total charge [%]
$SLEV$	slurry level in sump [m]

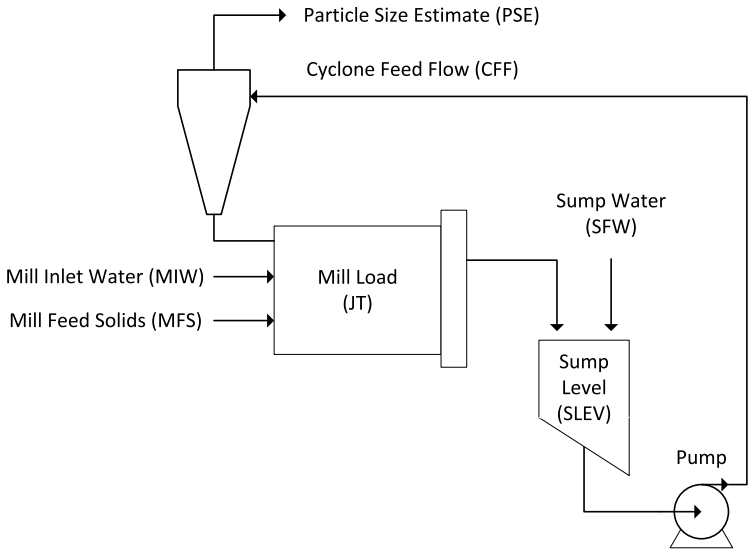

Figure 3.1: A single-stage closed circuit grinding ball mill.

3.3.1 Mill model

For the cumulative rates model particle sizes are reported as the cumulative percentage of ore smaller than size x_i (mm). The first and largest size x_1 is selected to be larger than the largest particles likely to be encountered in the feed stream. The sink size class n represents all particles with sizes between zero and x_n (Hinde and Kalala, 2009).

The specific cumulative breakage rate function K_i is the fractional rate at which particles above a given size x_i in the mill break to below that size per unit time. The energy-normalised cumulative breakage rate function is given by $K_i^E = (M/P) \cdot K_i$ and is generally insensitive to scale-up (Amestica et al., 1993). M (t) is the ore hold-up in the mill and P (kW) is the net mill power. The unit for K_i^E is $[\text{kWh/t}]^{-1}$.

The mill model considers a continuously fed mill and treats it as a single fully mixed reactor. The population balance equation with respect to time for size class 1 is:

$$\frac{dw_1}{dt} = f_1 - g_1 w_1 - w_1 \frac{P}{M} K_2^E \tag{3.1}$$

where w_i (t) is the absolute mass retained in size class i, f_i (t/h) is the absolute mass flow-rate for the mill feed for size class i and g_i (h^{-1}) is the specific discharge rate for size class i. Since there are no

Table 3.2: Nomenclature for cumulative rates model (1)

Parameter	Description
	Mill Parameters
α_{speed}	Fraction of critical mill speed
D	Inside diameter of mill [m]
ε_c	Effective porosity of the charge
f_0	Absolute mass flow of water in the feed stream [t/h]
f_i	Absolute mass flow of ore in size class i in the feed stream [t/h]
g_0	Specific discharge rate for water [h^{-1}]
g_i	Specific discharge rate for size class i [h^{-1}]
g_{max}	Specific discharge rate for water and ore sizes up to x_m [h^{-1}]
J_T	Static fractional volumetric filling for total charge
J_B	Static fractional volumetric filling of mill for balls
K_i^E	Energy-normalised cumulative breakage rate function of ore above size x_i [kWh/t]$^{-1}$
L	Inside length of mill [m]
M	Ore hold-up [t]
P_{mill}	Net mill power [kW]

particles larger than x_1, K_1^E is undefined and K_2^E is used in eq. (3.1) to describe the breakage of ore in size class 1 to smaller sizes.

The rate of change of the hold-up of material coarser than x_i is given by:

$$\frac{dW_i}{dt} = F_i - G_i - W_i \frac{P}{M} K_i^E \tag{3.2}$$

where W_i (t) is the mass of material coarser than size x_i inside the mill, F_i and G_i (t/h) are the cumulative mass flow-rates of material coarser than size x_i for the mill feed and product streams respectively.

A similar equation to eq. (3.2) can be constructed for material coarser than x_{i+1}:

$$\frac{dW_{(i+1)}}{dt} = F_{i+1} - G_{i+1} - W_{i+1} \frac{P}{M} K_{i+1}^E \tag{3.3}$$

The accumulation of material within size x_i $(i = 2, 3, ..., n-1)$ is given by the difference between eq.

Table 3.3: Nomenclature for cumulative rates model (2)

Parameter	Description
	Mill Parameters
ρ_B	Density of balls [t/m^3]
ρ_S	Density of ore [t/m^3]
v_{mill}	Internal mill volume [m^3]
w_0	Absolute mass of water in the mill [t]
w_b	Mass of balls inside the mill [t]
w_c	Weight of ore expressed as a fraction of the total mass of ore and water in the mill
w_i	Absolute mass of ore retained in size class i in the mill [t]
x_g	Effective mesh size of the grate above which discharge is zero [mm]
x_i	Size of size class i [mm]
ϕ	Volume percentage solids in the cyclone feed slurry
r_i	Flow-rate of material in size class i into the sump [m^3/h]
s_0	Flow-rate of water out of the sump [m^3/h]
s_i	Flow-rate of material in size class i out of the sump [m^3/h]
v_{pulp}	Total volume of slurry in the sump [m^3]

(3.3) and eq. (3.2):

$$\frac{dw_i}{dt} = f_i - g_i w_i + \left\{ W_i \frac{P}{M} K_i^E - (w_i + W_i) \frac{P}{M} K_{i+1}^E \right\} \tag{3.4}$$

The mass balance for particles in the sink size class n is:

$$\frac{dw_n}{dt} = f_n - g_n w_n + W_n \frac{P}{M} K_n^E \tag{3.5}$$

The water mass balance is given by:

$$\frac{dw_0}{dt} = f_0 - g_0 w_0 \tag{3.6}$$

where the flow of water into the mill is f_0 (m^3/h), the hold-up of water in the mill is w_0 (m^3) and the discharge rate of water out of the mill is g_0 (h^{-1}).

The final cumulative breakage rate population balance model for the grinding mill is given by eqs. (3.1), (3.4), (3.5) and (3.6).

3.3.1.1 Breakage rate function

Although it should be possible to measure the specific breakage rate function directly by means of radioactive tracer techniques, it is difficult and impractical. Rather, it is assumed that the breakage rate function can be represented by a simple equation with parameters that can be back-calculated from sampling campaign data (Austin and Klimpel, 1984; Hinde and Kalala, 2009).

At steady-state, the derivatives of eq. (3.1), (3.4) and (3.5) are zero and the specific cumulative breakage rate function values can be determined from the remaining variables which can be measured on a plant or pilot plant:

$$K_2^E = \frac{f_1 - g_1 w_1}{w_1 \frac{P}{M}} \tag{3.7}$$

$$K_{i+1}^E = \frac{f_i - g_i w_i + W_i \frac{P}{M} K_i^E}{(w_i + W_i)\frac{P}{M}};\ i = 2,3,...,n-1 \tag{3.8}$$

$$K_n^E = \frac{f_n - g_n w_n}{w_n \frac{P}{M}} \tag{3.9}$$

Once K_i^E has been determined for all size classes $(i = 2,3,...,n)$, the values can be fitted to the following equation from Hinde and Kalala (2009):

$$\hat{K}_i^E = \kappa_1 \left(\frac{x_i^{\alpha_1}}{1 + (x_i/\mu)^{\lambda}} + \kappa_2 x_i^{\alpha_2} \right)\ ;\ i = 2,3,...,n \tag{3.10}$$

where κ_1, κ_2, α_1, α_2, μ and λ are model parameters to be fitted.

3.3.1.2 Discharge rate function

The discharge rate function, which describes the rate at which slurry passes through the discharge grate, can be approximated by:

$$\begin{aligned} g_i &= g_{max}\ ;\ x_i \leq x_m \\ g_i &= g_{max} \frac{\ln x_i - \ln x_g}{\ln x_m - \ln x_g}\ ;\ x_m < x_i \leq x_g \\ g_i &= 0\ ;\ x_i > x_g \end{aligned} \tag{3.11}$$

where g_{max} (h^{-1}) is the specific discharge rate for water and fines up to size x_m. Size x_g is the effective mesh size of the grate above which discharge is zero.

3.3.1.3 Power draw function

The power draw of the mill is a function of the hold-up of water, ore and grinding media in the mill. A number of models are available in literature to estimate the power draw of SAG mills (Austin, 1990; Morrell, 2004). The cumulative rates model as described in Hinde and Kalala (2009) makes use of the power draw model of Austin (1990), which will also be used in this study:

$$P = 10.6D^{2.5}L(1-1.03J_T)\left(1-\frac{0.1}{2^{9-10\alpha_{speed}}}\right)\alpha_{speed}\cdot \left[(1-\varepsilon_c)\left(\frac{\rho_S}{w_c}\right)J_T + 0.6J_B\left(\rho_B-\frac{\rho_S}{w_c}\right)\right] \tag{3.12}$$

where J_T and J_B are the static fractional volumetric filling of the mill for the total charge and for the balls respectively, ε_c is the porosity of the charge, w_c is the weight of ore expressed as a fraction of the total mass of ore and water in the mill, ρ_B and ρ_S (t/m^3) are the density of the balls and the density of the ore respectively, α_{speed} is the mill speed expressed as a fraction of the critical speed and D and L (m) are the internal diameter and length of the mill respectively.

The static fractional volumetric filling of the mill for the total charge J_T can be approximated by:

$$J_T = \left(\frac{w_b}{\rho_B}+\frac{M}{\rho_S}+\frac{\varepsilon_c}{1-\varepsilon_c}\left(\frac{w_b}{\rho_B}+\frac{M}{\rho_S}\right)\right)/v_{mill} \tag{3.13}$$

where w_b (t) is the mass of balls and v_{mill} (m^3) is the internal volume of the mill.

3.3.2 Sump model

The sump is treated as a perfectly mixed vessel and the residence time in the piping and hydrocyclone is small compared to that of the sump. The accumulation of material in the sump is given by the difference in input and output flows:

$$\frac{dz_i}{dt} = r_i - s_i = r_i - \frac{CFFz_i}{v_{pulp}} \tag{3.14}$$

where z_i (m^3) is the volume of material in size class i in the sump, r_i (m^3/h) is the flow-rate of material in size class i into the sump, s_i is the flow-rate of material in size class i out of the sump, v_{pulp} (m^3) is the total volume of slurry in the sump and CFF (m^3/h) is the cyclone feed flow.

The flow-rate of water out of the sump s_0 is given by:

$$s_0 = CFF(1-\phi/100) \tag{3.15}$$

where ϕ is the volume percentage solids in the cyclone feed slurry.

3.3.3 Hydrocyclone model

The hydrocyclone model used in this study is the Plitt model with the equation for water split, as shown in Nageswararao et al. (2004). The Plitt model is commonly used to model hydrocyclones because it provides a complete process description as a function of common process variables. However, this model cannot accommodate high recoveries of solids to underflow as well as wide variations in feed size. Also, changes in the cyclone feed solids concentration and size distribution have a severe impact on the performance of the hydrocyclone. Care should be take when extrapolating this model outside the range of conditions used to estimate the model parameters. If the Plitt model uses parameters determined from pilot plant tests, the model cannot be guaranteed to operate correctly on industrial scale (Napier-Munn et al., 1999).

3.4 MODEL REDUCTION

The largest size class set considered in this study to model the grinding mill circuit by means of the cumulative rates model is 25 size classes. It is assumed that 25 size classes give a more accurate representation of the ore distribution and the non-linear cumulative breakage rate function K_i^E than fewer size classes. Therefore, the cumulative rates model with 25 size classes is the reference model against which models with smaller size class sets are compared. The reference size class set is named 25(Ref).

The smallest size class considered is $x_n = 75$ μm. This size class is increased 25 times by a factor of $\sqrt{2}$, the usual difference in aperture size for sieves (Stanley, 1987), until the largest size class $x_1 =$ 307.2 mm is reached. The sizes in set 25(Ref) can be seen in the first column of Table 3.4.

A large set of size classes can be reduced by lumping size classes together with a constant factor separating sizes. If size class set 25(Ref) is reduced in this manner to 9 size classes where the largest size remains $x_1 = 307.2$ mm and the smallest $x_n = 75$ μm, the sizes differ by a factor of $(\sqrt{2})^3$. For 5 size classes the sizes differ by $(\sqrt{2})^6$, and for 3 size classes by $(\sqrt{2})^{12}$. These three reduced size class sets are shown in Table 3.4 and are called $9l$, $5l$ and $3l$ respectively. The l indicates that the sizes in the reduced sets are log-linearly distributed.

The parameter values for the breakage rate function in eq. (3.10) are shown in Table 3.5. These parameter values were estimated in an optimisation study based on the cumulative rates model of an

Table 3.4: Size class sets in [mm] (*l*: Log-Linear Separation; *c*: Chosen Separation)

#	25(Ref)	9*l*	9*c*	5*l*	5*c*	3*l*	3*c*
1	307.2	307.2	307.2	307.2	307.2	307.2	307.2
2	217.2						
3	153.6		153.6				
4	108.6	108.6					
5	76.8						
6	54.3		54.3		54.3		
7	38.4	38.4	38.4	38.4			
8	27.2						
9	19.2						
10	13.6	13.6					
11	9.6						
12	6.8						
13	4.8	4.8		4.8		4.8	
14	3.4						
15	2.4						
16	1.7	1.7	1.7				
17	1.2						
18	0.85				0.85		
19	0.60	0.6	0.6	0.6			0.6
20	0.42						
21	0.30		0.3				
22	0.21	0.21			0.21		
23	0.15		0.15				
24	0.106						
25	0.075	0.075	0.075	0.075	0.075	0.075	0.075

Table 3.5: Breakage rate and Rosin-Rammler function parameters

Parameter	Value	Uncertainty
κ_1	1.13	5%
κ_2	3.0e-6	5%
α_1	1.11	5%
α_2	2.55	3%
λ	1.16	5%
μ	0.33	3%
β	0.36	20%
$D_{63.2}$	41.1	20%

industrial plant (Hinde, 2009). The cumulative breakage rate function K_i^E in eq. (3.10) represented by the three aforementioned size class sets is shown in Fig. 3.2a. From this figure it can be seen that size class sets $5l$ and $3l$ do not capture the non-linearity of $\log(K_i^E)$ below size 0.85 mm and above size 38.4 mm. Since K_1^E is undefined (see eq. (3.1)), only $n-1$ points appear in Fig. 3.2 when K_i^E is represented with n size classes.

The sizes in the reduced size class sets do not need to be log-linearly distributed. Reduced size class sets can be specified in such a way that the shape of K_i^E remains well defined by the sizes in the size class sets excluding the largest size x_1. Thus, three new reduced size class sets of 9, 5 and 3 sizes are chosen such that the non-linear nature of the breakage rate function is captured as best possible. The sizes in these three sets are chosen from the sizes in the reference set 25(Ref). The breakage rate function rather than the distribution of the mill charge is used to choose the smaller size class sets. The mill charge is a function of the breakage rate function and will reflect the shape of the breakage rate function. The three new reduced size class sets are shown in Table 3.4 and are called $9c$, $5c$ and $3c$. The c indicates that the size classes where chosen to best fit K_i^E. The procedure to choose these sizes is described below.

The reference size class set 25(Ref) consists of $N = 25$ size classes and is represented by $X = \{307.2, 217.2, ..., 0.075\}$ mm. For the reduced size class set S of M sizes, the largest size class is $x_1 = s_1 = 307.2$ mm and the smallest is $x_{25} = s_M = 75$ μm. Thus, there remains $M-2$ sizes to choose from set X to complete set S. The set m contains the size class numbers from set X included in the reduced size class set S, e.g. if $M = 3$, then $m = \{1, 19, 25\}$ and $S = \{307.2, 0.6, 0.075\}$ mm. The

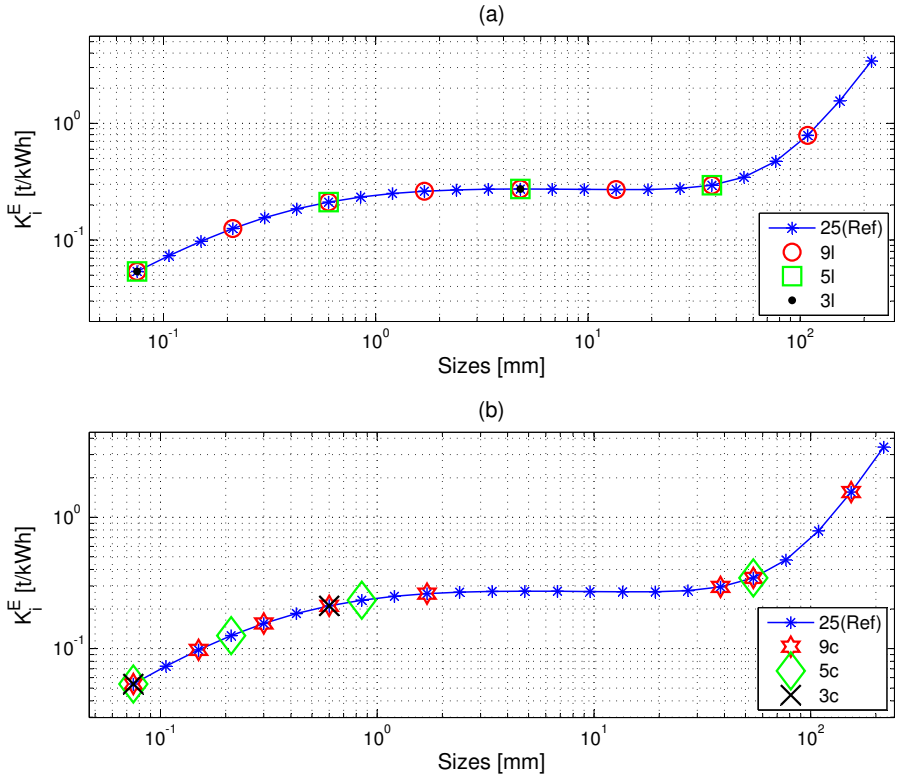

Figure 3.2: (a) Cumulative breakage rate function represented by the reference size class set 25(Ref) and the reduced size class sets $9l$, $5l$ and $3l$. The sizes in the latter three sets are distributed log-linearly. (b) Cumulative breakage rate function represented by the reference size class set 25(Ref) and the reduced size class sets $9c$, $5c$ and $3c$. The sizes in the latter three sets were chosen to best represent the non-linearity of the curve $\log K_i^E$.

function f below determines the squared sum of the distances between the curve $\log(K_i^E)$ represented by the 25 size classes in set X and straight lines connecting the points on $\log(K_i^E)$ represented by the M size classes in set S. In other words, function f determines the distance between $\log(K_i^E)$ represented by set X and the straight line approximation of $\log(K_i^E)$ with $M-1$ lines. The combination of sizes that gives the minimum value of function f is regarded as the best representation of K_i^E by M size classes:

$$f = \sum_{j=2}^{M-1} \sum_{i=m(j)+1}^{m(j+1)-1} \left[\log K_i^E - \log K_{m(j+1)}^E - \frac{\log K_{m(j)}^E - \log K_{m(j+1)}^E}{X_{m(j)} - X_{m(j+1)}} \left(X_i - X_{m(j+1)}\right)\right]^2$$
$$+ \sum_{k=3}^{m(2)-1} \left[\log K_k^E - \log K_{m(2)}^E - \frac{\log K_2^E - \log K_{m(2)}^E}{X_2 - X_{m(2)}} \left(X_k - X_{m(2)}\right)\right]^2 \tag{3.16}$$

The representation of the breakage rate function by size class sets $9c$, $5c$ and $3c$ is shown in Fig. 3.2b.

3.5 SYSTEM IDENTIFICATION

The seven size class sets shown in Table 3.4 are used to create seven non-linear cumulative rates models. These non-linear models are all linearized around the same operating point by means of a standard system identification procedure (Soderstrom and Stoica, 1989). The seven linear models are used to design seven separate linear model predictive controllers to control the grinding mill circuit shown in Fig. 3.1 as represented by the non-linear cumulative rates containing the reference set of 25 size classes. The performance of each controller should give an indication of the accuracy of the model used to design the controller.

3.5.1 Parameter values and operating point

The cumulative rates model parameter values are shown in Table 3.6. The operating point of the circuit during linearization is shown in Table 3.7. The model parameters and circuit's operating point was determined during the optimisation study of Hinde (2009).

The cumulative distribution of the solids feed and the cumulative distributions of the hold-up of ore in the mill and sump during linearization are shown in Fig. 3.3. The cumulative distribution of the solids feed to the mill is given by the truncated Rosin-Rammler distribution function:

$$P_{RR}(\bar{x}) = 1 - \exp\left(-\left(\frac{\eta}{\eta_{63.2}}\right)^{\beta}\right) \tag{3.17}$$

where $\eta = \frac{\varepsilon}{1-\varepsilon}$ and $\varepsilon = \bar{x}/x_1$. The largest size class is given by x_1, the vector containing all size classes from 1 to 25 is $\bar{x}$ and the measure of the spread in particle sizes is given by β. The size $D_{63.2}$ is the size where the cumulative distribution of solids feed is at 63.2% of its maximum; therefore $\eta_{63.2} = \frac{D_{63.2}/x_1}{1-D_{63.2}/x_1}$. The parameter values for this function are shown in Table 3.5. These parameter values were determined by fitting the Rosin-Rammler equation to the feed size distribution data from the report of Hinde (2009).

3.5.2 Linearized models

The System Identification Toolbox[1] in MATLAB was used to linearize the non-linear cumulative rates model for each of the seven different size class sets. Randomized steps of 10 h each for 120 h around the operating point of the circuit was used to fit each non-linear model to the 12 elements in

[1] System Identification Toolbox^{TM} is a registered trademark of The Mathworks, Inc.

Table 3.6: Grinding mill circuit parameters

Parameter	Description	Value	Unit
α_c	Fraction of critical mill speed	0.71	-
D	Internal mill diameter	4.20	m
ε_c	Charge porosity	0.3	-
g_{max}	Specific discharge rate for water and fines	27.5	h^{-1}
J_B	Static fractional volumetric filling of the mill for balls	0.24	-
L	Internal mill length	4.27	m
ρ_s	Ore density	3.2	t/m^3
ρ_b	Ball density	7.85	t/m^3
v_{mill}	Mill internal volume	59.12	m^3
w_b	Ball mass in the mill	66.8	t
x_g	Effective mesh size of grate for zero discharge	12	mm
x_m	Maximum fines size in discharge rate function	1	mm

Table 3.7: Operating point, variable constraints and MPC weights

Variable	Min	Max	OP	Weight	Unit
Manipulated Variables					
CFF	100	450	288	1.8e-7	m^3/h
MFS	0	150	69	1.0e-6	t/h
SFW	0	200	90	5.6e-7	m^3/h
MIW	0	20	3.7	5.6e-3	m^3/h
Controlled Variables					
PSE	0.5	0.85	0.69	1.75	Fraction
JT	0.2	0.5	0.32	8.3e-2	Fraction
$SLEV$	0.2	2	0.92	1	m
P_{mill}	-	-	1095	-	kW

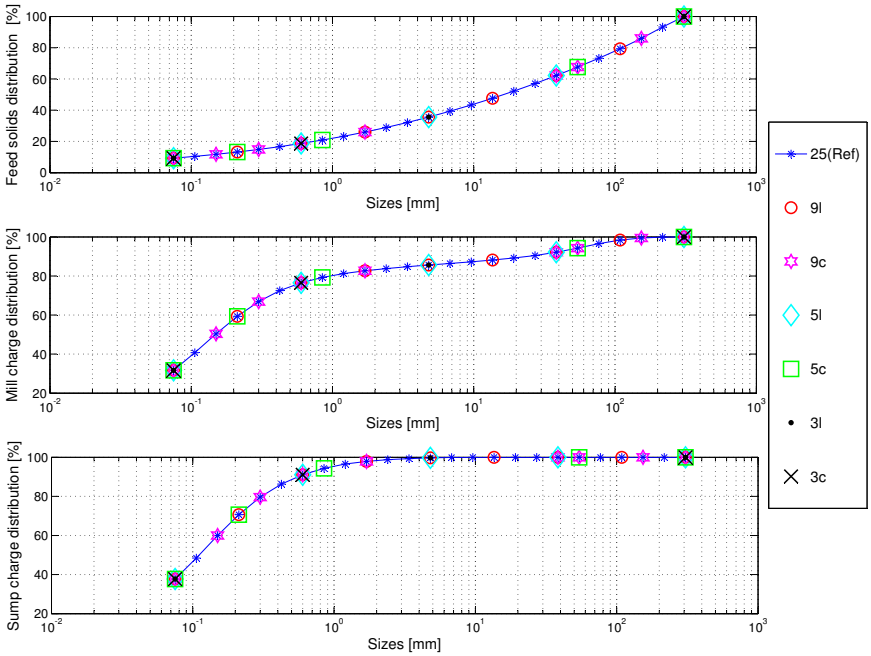

Figure 3.3: Cumulative distribution for solids feed, mill charge and sump charge represented by 25, 9, 5 and 3 size classes. (Ref - the reference size class set, *l* - size classes are log-linearly separated, *c* - separation between size classes is chosen.)

the transfer function matrix below:

$$\begin{bmatrix} PSE \\ JT \\ SLEV \end{bmatrix} = \begin{bmatrix} G_{11} & G_{12} & G_{13} & G_{14} \\ G_{21} & G_{22} & G_{23} & G_{24} \\ G_{31} & G_{32} & G_{33} & G_{34} \end{bmatrix} \begin{bmatrix} CFF \\ MFS \\ SFW \\ MIW \end{bmatrix} \tag{3.18}$$

The transfer function elements in eq. (3.18) are:

$$G_{11} = \frac{K\left(sT_z+1\right)}{\left(sT_{p1}+1\right)\left(sT_{p2}+1\right)}e^{-T_d s} \tag{3.19}$$

$$G_{12-14,21,23,24} = \frac{K}{sT_p+1}e^{-T_d s} \tag{3.20}$$

$$G_{22} = \frac{K}{sT_p+1} \tag{3.21}$$

$$G_{31,33} = \frac{K}{s} \tag{3.22}$$

$$G_{32,34} = \frac{K}{s}e^{-T_d s} \tag{3.23}$$

Table 3.8: Transfer function parameters of log-linearly distributed size class sets (1)

Function		Size class set			
PSE		25(Ref)	9*l*	5*l*	3*l*
	K	-1.7e-3	-1.7e-3	-2.2e-3	-3.4e-3
G_{11}	$Tp1$	0.84	0.87	0.89	2.4
-	$Tp2$	4.3e-2	5.5e-4	0.3	-
CFF	Tz	-0.16	-0.19	-0.05	-
	Td	0.01	0.01	0.01	0.01
G_{12}	K	-3.7e-3	-3.8e-3	-4.4e-3	-5.5e-3
-	Tp	0.76	0.75	0.74	1.9
MFS	Td	0.05	0.05	0.05	0.05
G_{13}	K	4.0e-3	4.1e-3	5.2e-3	8.9e-3
-	Tp	0.96	0.97	0.96	2.8
SFW	Td	0.01	0.01	0.01	0.01
G_{14}	K	4.1e-3	4.2e-3	5.4e-3	0.01
-	Tp	0.41	0.40	0.35	2.0
MIW	Td	0.02	0.02	0.02	0.02
JT		25(Ref)	9*l*	5*l*	3*l*
G_{21}	K	5.0e-4	5.1e-4	5.3e-4	2.1e-3
-	Tp	0.27	0.28	0.24	1.4
CFF	Td	0.01	0.01	0.01	0.01
G_{22}	K	1.1e-3	1.1e-3	1.1e-3	3.3e-3
MFS	Tp	0.30	0.29	0.26	1.2

where K is a proportional gain, T_d is a time delay, T_p is a pole time constant and T_z is a zero time constant.

Tables 3.8-3.9 and 3.10-3.11 show the values of the transfer function parameters for the log-linear and the chosen size class set distributions respectively. The time delays and the time constants are given in hours. The inputs to the transfer functions have not been normalized. The linearized model of the circuit modelled with 25 size classes is regarded as the reference model.

Table 3.9: Transfer function parameters of log-linearly distributed size class sets (2)

Function		Size class set			
JT		25(Ref)	9*l*	5*l*	3*l*
G_{23}	K	-5.1e-4	-5.1e-4	-4.6e-4	-2.1e-3
-	Tp	0.91	0.93	1.1	1.4
SFW	Td	0.02	0.02	0.02	0.02
G_{24}	K	-5.3e-4	-5.4e-4	-4.8e-4	-2.6e-3
-	Tp	0.39	0.40	0.44	1.3
MIW	Td	0.05	0.05	0.05	0.05
SLEV		25(Ref)	9*l*	5*l*	3*l*
G_{31}	K	-0.13	-0.13	-0.13	-0.12
G_{32}	K	0.11	0.11	0.11	0.11
MFS	Td	0.1	0.1	0.1	0.1
G_{33}	K	0.25	0.25	0.25	0.23
G_{34}	K	0.25	0.25	0.25	0.23
MIW	Td	0.04	0.04	0.04	0.04

Tables 3.8-3.9 show very little difference between the transfer function parameter values for reference set 25(Ref) and size class set 9*l*. A larger difference in transfer function parameter values occurs between size class set 25(Ref) and size class set 5*l*. For Tables 3.10-3.11 the difference between the transfer function parameter values for set 25(Ref) and size class sets 9*c* and 5*c* are very small.

The response of the circuit modelled with size class set 3*l* could not be fitted to the transfer function shown in eq. (3.19). For the linearized model of this size class set, a first order plus time delay transfer function was used. As shown in Tables 3.8-3.9, the gains of the linearized model for set 3*l* are all in the correct directions, but differ significantly in magnitude from the gains of the model for the reference set 25(Ref). In contrast to set 3*l*, the difference in transfer function parameter values between the linear model of set 25(Ref) and the linear model of set 3*c* is much smaller.

For the sump level (*SLEV*), the transfer function parameter values are almost identical irrespective of the size class set.

Table 3.10: Transfer function parameters of chosen size class sets (1)

Function		Size class set			
PSE		25(Ref)	9*c*	5*c*	3*c*
	K	-1.7e-3	-1.7e-3	-1.7e-3	-2.1e-3
G_{11}	$Tp1$	0.84	0.80	0.81	0.81
-	$Tp2$	4.3e-2	4.4e-4	6.3e-4	0.27
CFF	Tz	-0.16	-0.17	-0.18	-0.06
	Td	0.01	0.01	0.01	0.01
G_{12}	K	-3.7e-3	-3.8e-3	-3.8e-3	-4.4e-3
-	Tp	0.76	0.65	0.67	0.61
MFS	Td	0.05	0.05	0.05	0.05
G_{13}	K	4.0e-3	4.0e-3	4.0e-3	5.1e-3
-	Tp	0.96	0.85	0.88	0.77
SFW	Td	0.01	0.01	0.01	0.01
G_{14}	K	4.1e-3	4.1e-3	4.1e-3	5.3e-3
-	Tp	0.41	0.34	0.27	0.28
MIW	Td	0.02	0.02	0.02	0.02
JT		25(Ref)	9*c*	5*c*	3*c*
G_{21}	K	5.0e-4	5.1e-4	5.3e-4	5.4e-4
-	Tp	0.27	0.30	0.33	0.32
CFF	Td	0.01	0.01	0.01	0.01
G_{22}	K	1.1e-3	1.1e-3	1.2e-3	1.2e-3
MFS	Tp	0.30	0.26	0.26	0.23

3.6 MODEL PREDICTIVE CONTROL

The main challenges when controlling a grinding process are the strong coupling between variables, the existence of large time delays, the variation of parameters over time and the non-linearities in the process. Model Predictive Control (MPC) is ideal for the grinding process because it has the ability to handle pairing problems in multivariable systems, to handle processes with large time delays and to impose constraints on manipulated and controlled variables. The disadvantages of a MPC scheme

Table 3.11: Transfer function parameters of chosen size class sets (2)

Function		Size class set			
JT		25(Ref)	9*c*	5*c*	3*c*
G_{23}	K	-5.1e-4	-5.1e-4	-5.3e-4	-4.4e-4
-	Tp	0.91	0.80	0.80	0.98
SFW	Td	0.02	0.02	0.02	0.02
G_{24}	K	-5.3e-4	-5.3e-4	-5.5e-4	-4.7e-4
-	Tp	0.39	0.34	0.31	0.32
MIW	Td	0.05	0.05	0.05	0.05
SLEV		25(Ref)	9*c*	5*c*	3*c*
G_{31}	K	-0.13	-0.13	-0.13	-0.13
G_{32}	K	0.11	0.11	0.11	0.11
MFS	Td	0.1	0.1	0.1	0.1
G_{33}	K	0.25	0.25	0.25	0.25
G_{34}	K	0.25	0.25	0.25	0.25
MIW	Td	0.04	0.04	0.04	0.04

are the computational burden for large processes with long control and prediction horizons, the dependency on a reliable and accurate process model and the deterioration in controller performance in the presence of strong external disturbances (Chen et al., 2009).

The study of Ramasamy et al. (2005) indicated improvements in the performance of a laboratory grinding mill circuit controlled by means of a MPC scheme compared to a multi-loop detuned PI(D) control scheme. MPC has also been successfully used to control industrial grinding mill circuits (Chen et al., 2007, 2008; Wei and Craig, 2009b). A survey of commercial MPC technologies can be found in Qin and Badgwell (2003).

3.6.1 Overview

A linear MPC scheme is a model-based control strategy that utilizes a linear model of the plant to predict future behaviour of the plant. At each sampling interval the controller attempts to calculate a series of C control moves that will optimize the future behaviour of the plant for the next P sampling

intervals. Because a new series of control moves is calculated at every sampling interval, only the first control move in the series is implemented. A performance index defines the optimal future behaviour of the plant and aims to prevent violations of manipulated and controlled variable constraints, to prevent excessive manipulated variable changes and to drive controlled variables to their optimal set-points (Qin and Badgwell, 2003).

The control action taken at time k is obtained by selecting an input sequence u that minimizes the scalar performance index J:

$$J(k) = \sum_{j=1}^{P} [\hat{y}(k+j) - r(k+j)]^T Q [\hat{y}(k+j) - r(k+j)]$$
$$+ \sum_{j=1}^{C} [\Delta u(k+j-1)]^T R [\Delta u(k+j-1)] \tag{3.24}$$

where $\hat{y}(k)$, $r(k)$ and $\Delta u(k)$ are the vectors of predicted outputs, set-point trajectories and changes in the inputs at time k respectively, P and C are the prediction and control horizon respectively, $Q = \text{diag}[q_1, q_2 ... q_P]$ and $R = \text{diag}[r_1, r_2 ... r_C]$ are the error and input weighting matrices respectively. The magnitude and rate constraints on the manipulated and controlled variables are given by:

$$\begin{aligned} u_{\min} \leq u(k) \leq u_{\max}, \quad k = 0, 1, ...C-1 \\ \Delta u_{\min} \leq \Delta u(k) \leq \Delta u_{\max}, \quad k = 0, 1, ...C-1 \\ y_{\min} \leq y(k) \leq y_{\max}, \quad k = 0, 1, ..., P-1 \end{aligned} \tag{3.25}$$

Tighter control of controlled variables can be achieved by choosing larger weights in matrix Q and excessive variations in manipulated variables can be avoided by choosing appropriate values for matrix R (Chen et al., 2007, 2008).

3.6.2 Controller design

The MPC Toolbox[2] of MATLAB was used to create seven controllers from the seven linearised plant models of the grinding mill circuit. All seven controllers use a sampling time of 10 s, a prediction horizon of 200 samples and a control horizon of 3 samples. The constraints imposed by the controller for each variable and the weights for the R and Q matrices in eq. (3.24) are shown in Table 3.7. The weighting matrices, calculated during the tuning of the controller, are shown below for further clarification:

$$Q = \text{diag}[1.75, 0.083, 1]; \quad R = \text{diag}[1.8\text{e-}7, 1.0\text{e-}6, 5.6\text{e-}7, 5.6\text{e-}3] \tag{3.26}$$

[2]Model Predictive Control Toolbox^{TM} is a registered trademark of The Mathworks, Inc.

It is important to note that the relative values of the Q and R weighting matrices and not the absolute values of these matrices determine the performance of the controller. Because the inputs and outputs of the models have not been scaled, the weights have been scaled according to the ranges of the manipulated variables. The controller aims to control the product particle size estimate (PSE) tightly, while allowing the fractional volumetric filling of the mill (JT) and the sump level ($SLEV$) to vary around their set-points and within their constraints. It is important to maintain JT and $SLEV$ within their constraints as these variables are open-loop unstable. The controller makes equal use of the manipulated variables cyclone feed flow-rate (CFF), feed-rate of solids to the mill (MFS) and flow-rate of water to the sump (SFW), but less use of the flow-rate of water to the mill (MIW) to drive the controlled variables to their set-points.

3.7 SIMULATION, RESULTS AND DISCUSSION

3.7.1 Simulation

A simulation platform was created in Simulink[3] to simulate the single-stage grinding mill circuit in Fig. 3.1 modelled by the non-linear cumulative rates model with 25 size classes. Each of the seven model predictive controllers was implemented on the non-linear model. Therefore, there are seven simulations where each simulation makes use of a different controller to control the non-linear model with 25 size classes. The performance of the controllers based on the reduced size class sets is compared to the performance of the controller based on the reference size class set of 25 sizes.

The equilibrium of a grinding mill is perturbed when the feed-rate, feed ore distribution or hardness varies. The effect of these variations on the behaviour of the grinding mill requires time to decay. Although it is desirable to manipulate all three of these variables, only feed-rate can be manipulated. A grinding mill circuit has to contend with the other two variables as disturbances. Changes in the feed hardness and size distribution will result in changes in the grinding media size distribution, which will affect the breakage characteristics in the mill (Napier-Munn et al., 1999; Coetzee et al., 2010).

During simulation, the feed ore distribution was altered every 13 h by randomly adjusting the Rosin-Rammler function parameters in eq. (3.17) according to the uncertainties shown in Table 3.5. The feed ore hardness was altered indirectly by adjusting the breakage rate function parameters in eq. (3.10)

[3] Simulink is a registered trademarks of The MathWorks Inc.

according to the uncertainties shown in Table 3.5 every 8 h. The parameters in both functions follow a uniform distribution where the minimum and maximum of the distribution are given by:

$$\min = p(1-\Delta_p/100); \;\; \max = p(1+\Delta_p/100) \tag{3.27}$$

where Δ is the uncertainty of parameter p. The uncertainties were chosen such that fairly large disturbances in the feed ore distribution and feed ore hardness could be simulated.

Measurement noise was added to the controlled variables: product particle size estimate (PSE), fractional volumetric filling of the mill (JT) and sump level ($SLEV$). The noise was normally distributed with a variance of 2% for $SLEV$ and a variance of 3% for PSE and JT. Given the ranges of the three controlled variables, the noise on PSE and JT is significantly larger than the noise on $SLEV$.

During simulation, the set-points for JT and $SLEV$ were kept constant. The set-point for PSE was adjusted every 20 h: $PSE = \{0.69, 0.64, 0.58, 0.62\}$.

3.7.2 Results and discussion

The manipulated variables for the feed-rate of ore to the mill (MFS), the flow-rate of water to the mill (MIW), the flow-rate of water to the sump (SFW) and the cyclone feed flow-rate (CFF) are shown in Figs. 3.4 and 3.5. All the controllers, except the controller based on size class set 3l, adjusted the manipulated variables at similar rates and degrees of magnitude.

The fraction of the mill filled (JT) is shown in Fig. 3.6, the sump level ($SLEV$) is shown in Fig. 3.7, the percentage of the cyclone overflow that passes -75 μm (PSE) is shown in Fig. 3.8, and the mill power draw is shown in Fig. 3.9. The figures indicate that the controller allowed JT and $SLEV$ to vary away from their set-points in order to have tight control of PSE.

Figures 3.6 to 3.9 show that the controllers based on reduced size class sets 9l, 9c and 5c cause the controlled variables to follow almost the exact same path as the controlled variables for the controller based on the reference size class set 25(Ref). This is to be expected since the linearized models for sets 25(Ref), 9l, 9c and 5c have almost identical transfer function parameter values.

Although the controllers based on reduced size class sets 5l and 3c do not cause the controlled variables to follow the exact same path as the controlled variables for the controller based on set 25(Ref), the rate and magnitude of changes remain similar. The figures indicate that controllers based on 5l

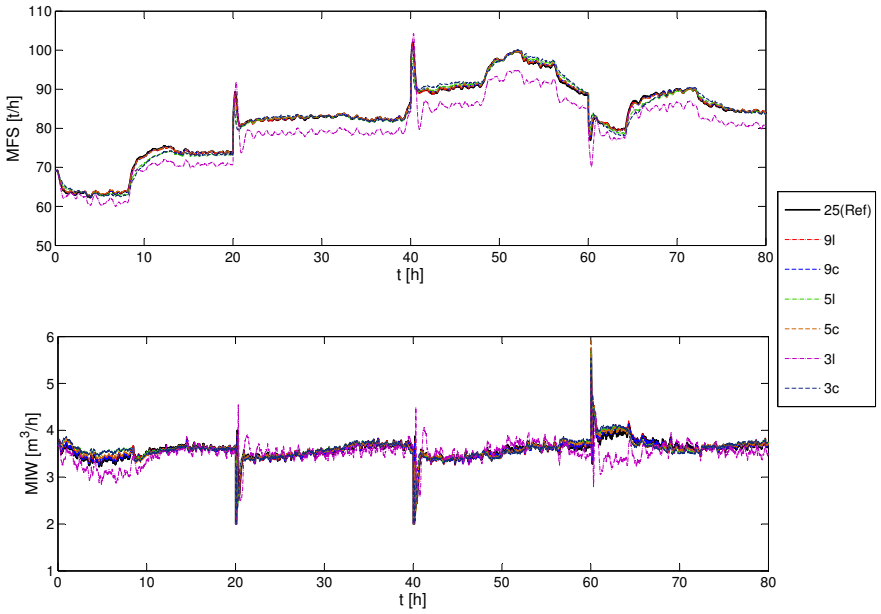

Figure 3.4: Manipulated variables MFS and MIW for each controller of the seven size class sets shown in Table 3.4.

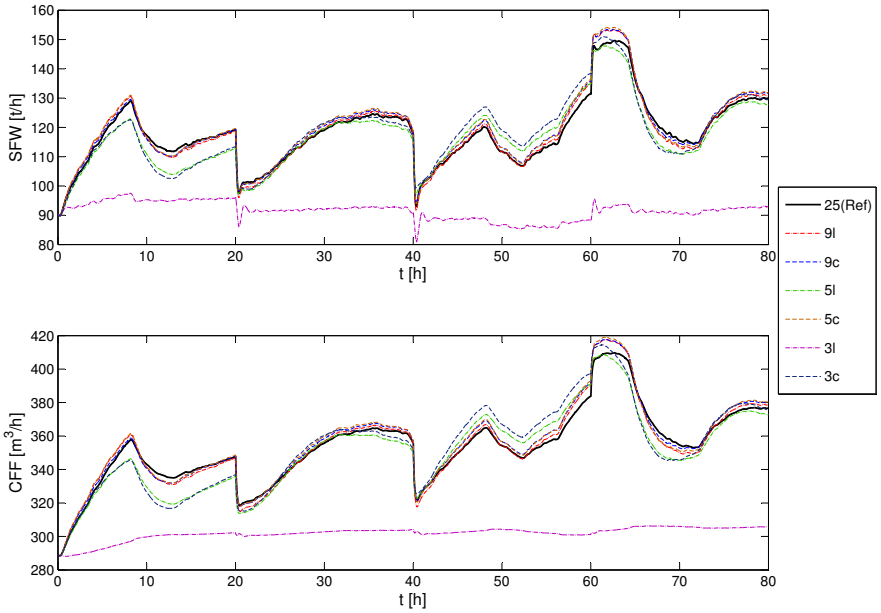

Figure 3.5: Manipulated variables SFW and CFF for each controller of the seven size class sets shown in Table 3.4.

and 3c are almost identical, which is to be expected since the linearized model parameters for these size class sets in Tables 3.8-3.9 and 3.10-3.11 are almost identical.

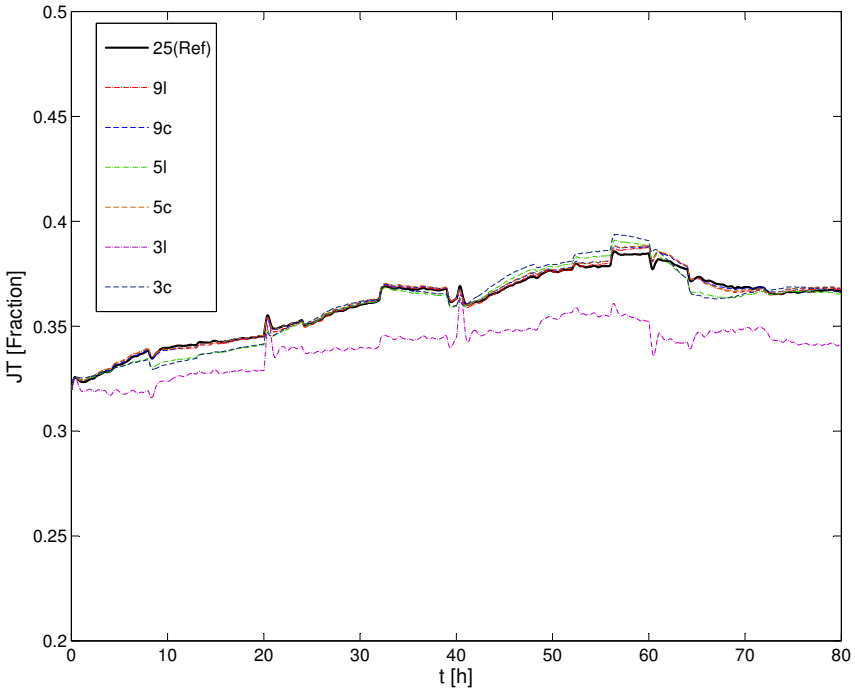

Figure 3.6: Simulation results of fractional volumetric filling (JT) of the mill for all size class sets.

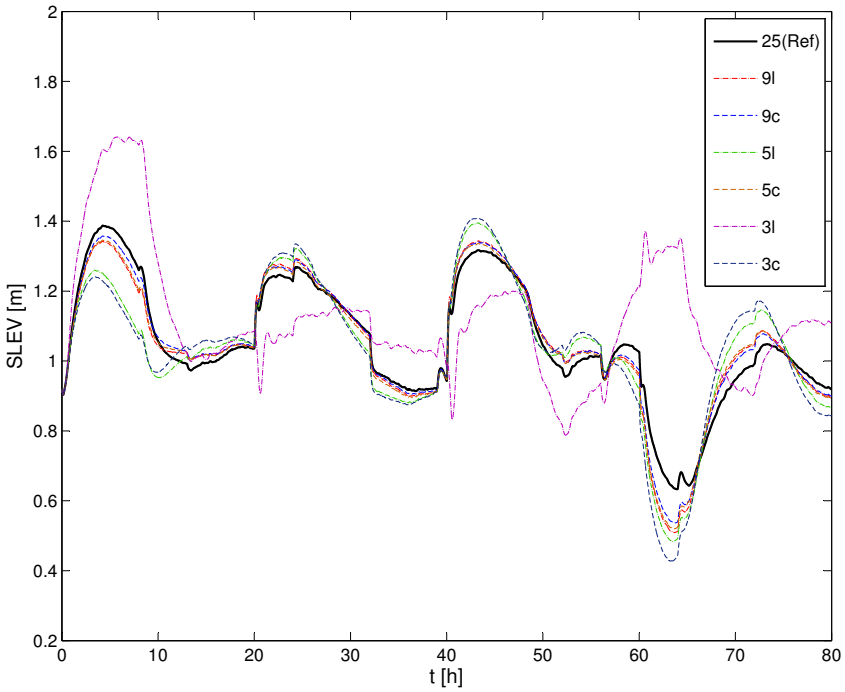

Figure 3.7: Simulation results of sump level ($SLEV$) for all size class sets.

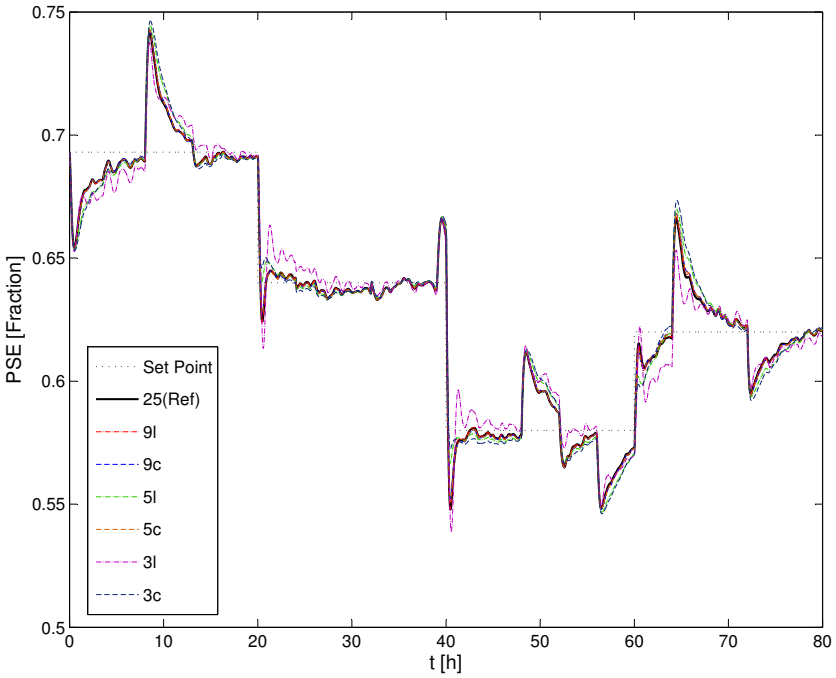

Figure 3.8: Simulation results of percentage of cyclone overflow that passes 75 μm (PSE) for all size class sets.

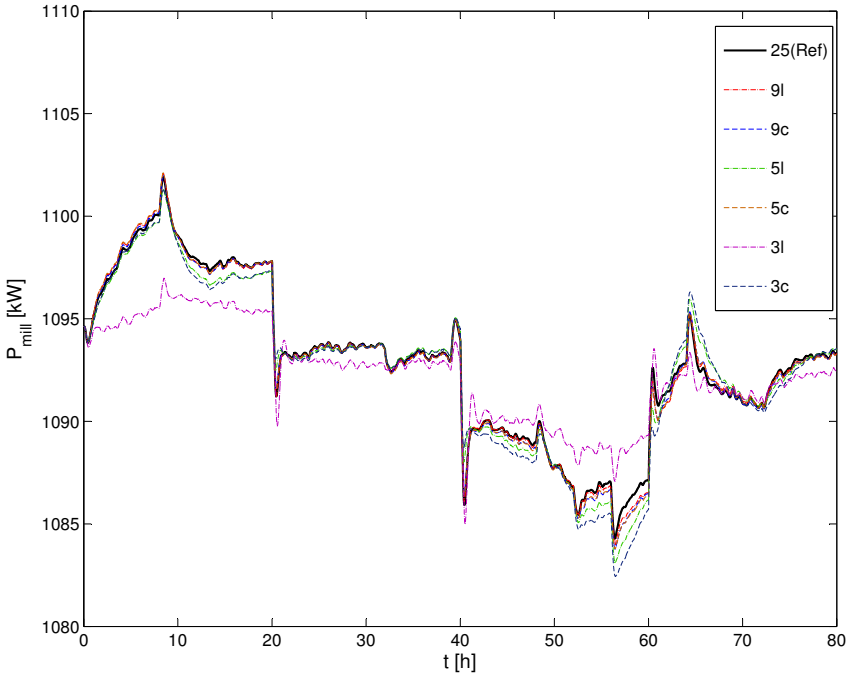

Figure 3.9: Simulation results of mill power draw (P_{mill}) for all size class sets.

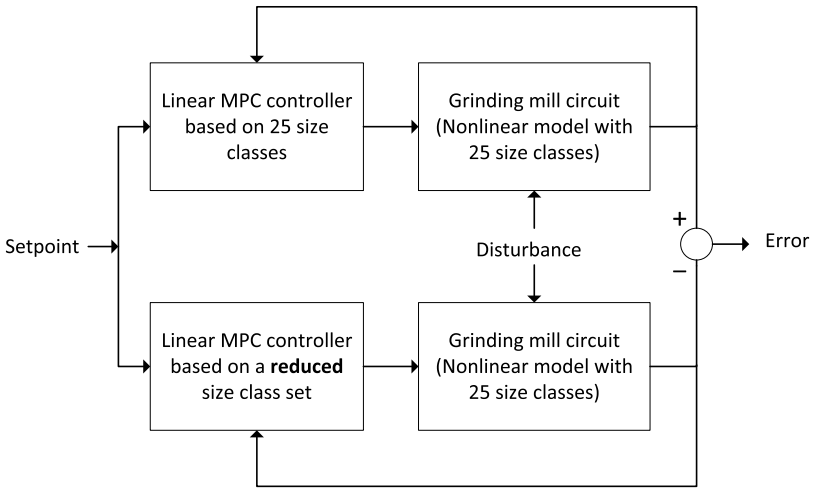

Figure 3.10: Illustration of simulation structure to evaluate controller performance.

The controller based on size class set 3*l* does not cause the controlled variables *JT* and *SLEV* to follow a similar path as the other controllers. Because *PSE* was given a high priority, the controller for set 3*l* is able control *PSE* in an almost identical fashion to the reference controller for set 25(Ref).

During the simulation, the feed ore hardness varies at intervals of 8 h and the feed ore distribution at intervals of 13 h. The first disturbance occurs at time 0 h, as seen in Fig. 3.8. This figure shows that the controller is not able to suppress large disturbances very quickly. The disturbances cause a mismatch between the plant and the model used by the controller. However, the controller is able to return *PSE* back to its set-point in the presence of the disturbances. It should be remembered that the size of the sump has an influence on the ability to reject disturbances in *PSE*. A large sump acts as a large buffer and provides more leeway to reject disturbances.

The analysis of the performance of the controllers is illustrated in Fig. 3.10. The difference between the controlled or manipulated variables of the circuit with the reference size class set controller and the same variables of the circuit with a reduced size class set controller can be quantified by means of the normalised root mean squared error (NRMSE) expressed as a percentage:

$$\%NRMSE = 100\left(\frac{\left\|y_{25(Ref)} - \hat{y}\right\|_2}{\left\|y_{25(Ref)} - mean(y_{25(Ref)})\right\|_2}\right) \tag{3.28}$$

where $y_{25(Ref)}$ is a time-signal for the reference size class set and $\hat{y}$ is a time-signal for a reduced size

Table 3.12: Percentage NRMSE between reference model and reduced models' controlled and manipulated variables

	$9l$ [%]	$9c$ [%]	$5l$ [%]	$5c$ [%]	$3l$ [%]	$3c$ [%]
CFF	13.9	15.0	36.1	17.8	251	43.9
MFS	2.25	3.15	10.4	3.24	39.5	13.7
SFW	14.2	15.7	36.6	18.4	257	44.1
MIW	17.6	20.1	53.2	33.9	107	64.5
PSE	0.91	1.95	8.01	1.73	12.9	10.4
JT	7.80	8.45	21.8	9.83	133	27.5
$SLEV$	23.9	18.9	44.1	23.0	120	55.2
P_{mill}	5.25	6.38	15.4	6.87	45.5	21.9

class set. The results of the comparison between signal 25(Ref) and the other signals in each of the Figs. 3.4-3.9 are shown in Table 3.12.

Table 3.12 affirms that the controllers for sets $9l$, $9c$ and $5c$ give approximately equal responses. These sets give a fairly accurate description of the grinding mill circuit modelled by 25 size classes. According to the table, the controller for set $5l$ is slightly more accurate than the controller for set $3c$. These two sets define models which are reasonably similar to the model of the grinding mill circuit with the reference set. Finally, set $3l$ cannot describe the grinding mill circuit as accurately as 25 size classes. Yet, because this set correctly indicates the direction each variable will change, the linear controller for this set is able to control the non-linear circuit modelled by 25 size classes.

3.8 CONCLUSION

When developing a grinding mill circuit model, it is important to clearly identify the aim of the model. A model with a large size class set provides valuable information for plant design and scale-up, whereas a simple model with a small size class set may be more suited for process control design (Laplante et al., 1987). This chapter focused on the effect that small size class sets have on the accuracy of a model for use in a process control system.

The computational burden of simulating a grinding mill circuit with 25 size classes is much greater than simulating the same circuit with fewer size classes. This is simply because more size classes

require more population balance equations to be solved in the cumulative rates model. If a reduced size class set is used in a non-linear MPC scheme, the minimization of the cost function should take less time because the time necessary to predict the future behaviour of the plant is reduced. An example where a reduced size class set was used in a robust nonlinear model predictive controller framework can be found in Coetzee et al. (2010). Even though a reduced size class set was used, the computational time was too long for the controller to be implemented on a plant in real-time. Yet, future processors should be able to handle non-linear models with large size class sets with ease since computational power should increase according to Moore's law.

If only a few size classes are used to characterize the inflow and outflow of each unit in the milling circuit, less sieves are required during a sampling campaign to obtain data to fit a model for process control. It is not necessary to construct special sieves for such a sampling campaign. A subset of available standard sieves can be used. Although this will reduce the sampling campaign time, it is possible that the sieves will not be able to handle the weight of slurry samples. A sampling campaign with only a few sieves will require careful planning to make sure that a representative slurry sample is used which the sieves will be able to handle.

When estimating the parameters of the cumulative breakage rate function in eq. (3.10), it is not necessary to use 25 size classes. As seen from the linearized models, when the cumulative breakage rate K_i^E is represented by a reduced size class set the model of the grinding mill circuit remains almost as accurate as the model with the full size class set. With fewer size classes calculation of the parameters in eq. (3.10) can be done more easily since more degrees of freedom are available to fit the function. However, if only a few size classes are used more care should be taken to ensure the size class set captures the non-linear behaviour of K_i^E. A poor representation of K_i^E will result in a deterioration of model accuracy.

For a reduced size class set, the sizes do not need to be log-linearly distributed. The cumulative rates model with 3 (or 5) size classes chosen according to the shape of the curve $\log K_i^E$, produced the same response as the cumulative rates model with 5 (or 9) size classes log-linearly distributed. (I.e. sets $3c$ and $5l$, and sets $5c$ and $9l$ produce almost identical model responses.) Therefore, a trade-off has to be made. More size classes ensures that any non-linear behaviour of the breakage rate is captured, but the sampling campaign requires more effort. It is therefore possible to do a sampling campaign for 9 size classes, but to use only a selection of 5 size classes to model the circuit.

The grinding mill circuit modelled with 3 size classes log-linearly distributed produced responses in the correct directions, but with incorrect magnitudes. Even though there was considerable mismatch between the plant model and the controller model, the model predictive controller was able to control *PSE* and maintain the other controlled variables within their constraints. This shows that even though a model may only give an estimate of the directions of changes in the controlled variables for changes in the manipulated variables, the model can still prove useful for control purposes.

CHAPTER 4

ANALYSIS AND VALIDATION OF A GRINDING MILL MODEL FOR PROCESS CONTROL

4.1 INTRODUCTION

The unique and novel grinding mill circuit model considered in this chapter uses the minimum number of states and parameters necessary for control and estimation purposes. The aim of the model is to provide a simple and theoretically sound model that can be easily implemented and maintained in an advanced process control system without having to resort to purely empirical models. There are potential economic benefits for the operation of grinding mill circuits if such a model is used (Bauer and Craig, 2008; Wei and Craig, 2009a).

Although the model described in this chapter has already been presented in Hulbert (2005) and Coetzee et al. (2010), both cases lacked a thorough description and validation of the model. The aim of this chapter is to present the underlying assumptions and basis of the model, describe how the model works and provide a step-wise procedure to fit the model to plant data. In the chapter the model is fitted to data from an actual full-scale plant and evaluated as to how well it reconciles with the sampling campaign plant data at various operating conditions. This chapter is an expanded version of le Roux et al. (2012). The model will be referred to as the *Hulbert*-model (after Hulbert (2005)) throughout the rest of the chapter.

4.2 THE *HULBERT*-MODEL

A SAG mill with an end-discharge screen in a single-stage closed circuit configuration, as shown in Fig. 4.1, is considered in this chapter. The manipulated and controlled variables in Fig. 4.1 are

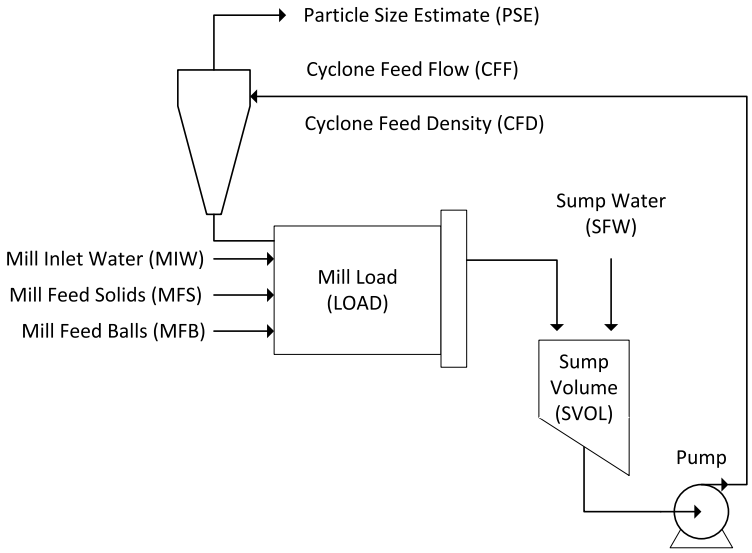

Figure 4.1: A single-stage closed circuit grinding mill.

Table 4.1: Description of circuit variables

Variable	Description
	Manipulated Variables
MIW	flow-rate of water to the mill [m^3/h]
MFS	feed-rate of ore to the mill [t/h]
MFB	feed-rate of steel balls to the mill [t/h]
SFW	flow-rate of water to the sump [m^3/h]
CFF	flow-rate of slurry to the cyclone [m^3/h]
	Controlled Variables
PSE	product particle size [%]
$LOAD$	volume of charge within the mill [m^3]
$SVOL$	volume of slurry in sump [m^3]

described in Table 4.1. A complete process description can be found in Chapter 2.

The circuit shown in Fig. 4.1 can be described by the reduced complexity non-linear model found in Hulbert (2005) and Coetzee et al. (2010). The approach in the derivation of this model was to use as few fitted parameters as possible while still making the model produce responses that are reason-

ably accurate and in the right direction. By minimising the number of parameters to fit, redundancy and unmeasurable or uncontrollable degrees of freedom are reduced. This tends to maximise the invertability of the model to obtain parameters from data.

Another aim was to make the model applicable over a wide range of operating regions. To do this, functional forms were made consistent with known physical requirements (e.g. mass conservation) and valid at extreme conditions (e.g. minimum water content in slurry). For example, the Plitt cyclone model can predict underflows with negative water concentrations. The functional form of the Plitt model does not include the useful information that it is impossible for any cyclone to squeeze water out of slurry below some volumetric percentage of water (Nageswararao et al., 2004). Phenomenological modelling is used to provide functional forms where appropriate, but not if it entails the use of more fitted parameters than are absolutely essential to produce the required characteristics.

The model consists of four modules: a feeder, a SAG mill with an end-discharge screen, a sump and a hydrocyclone classifier. All the modules, except for the feeder, can be seen in Fig. 4.1. The feeder is responsible for the feed of ROM ore, water, balls and the hydrocyclone underflow slurry to the mill. The function of the other three modules - the mill, the sump and hydrocyclone - is described in Chapter 2.

The model uses five states to represent the constituents of charge in the milling circuit. The states are rocks, solids, fines, balls and water. Rocks are ore too large to be discharged from the mill, whereas solids are ore that can be discharged from the mill. The solids consist of the sum of fine and coarse ore, where fine ore is smaller than the product specification size and coarse ore is larger than the product specification size. It is assumed that fines are essentially inseparable from the water found throughout the grinding mill circuit. Balls and rocks are only found in the mill, as they are too large to pass through the apertures in the end-discharge screen. The mill in the circuit is treated as a fully mixed reactor. The manipulated and controlled variables for the model can be seen in Table 4.1 and Fig. 4.1.

Each of the four modules and their mathematical descriptions are shown below. For the equations, V denotes a flow-rate in m^3/h and X denotes the states of the model as volumes in m^3. Table 4.2 provides a description of the subscripts for V and X. The first subscript indicates the module considered, the second subscript specifies which of the five states are considered and in the case of flow-rates the final subscript shows if it is an inflow, outflow or underflow. The nomenclature for the model is shown in

Table 4.2: Description of subscripts for the *Hulbert*-model

Subscript	Description
$X_{\Delta-}$	f-feeder; m-mill; s-sump; c-cyclone
$X_{-\Delta}$	w-water; s-solids; c-coarse; f-fines; r-rocks; b-balls; t-total
$V_{--\Delta}$	i-inflow; o-outflow; u-underflow

Table 4.3.

4.2.1 Feeder module

The feeder module divides the ore fed to the mill into various streams. Each stream represents the flow-rate of one of the five states out of the feeder module into the mill module: water (V_{fwo}), solids (V_{fso}), fines (V_{ffo}), rocks (V_{fro}) and balls (V_{fbo}). The flow-rates are defined as:

$$V_{fwo} = MIW, \tag{4.1}$$

$$V_{fso} = \frac{MFS}{D_S}(1-\alpha_r) \tag{4.2}$$

$$V_{ffo} = \frac{MFS}{D_S}\alpha_f \tag{4.3}$$

$$V_{fro} = \frac{MFS}{D_S}\alpha_r \tag{4.4}$$

$$V_{fbo} = \frac{MFB}{D_B} \tag{4.5}$$

The parameters α_f and α_r define the fraction of fines and rock respectively of the feed-rate of ore to the mill (MFS). By dividing the feed-rate of ore to the mill (MFS) and the feed-rate of balls to the mill (MFB) by the density of ore (D_S) and balls (D_B) respectively, the correct units are obtained. The implicit assumption when dividing by the ore density (D_S) in eq. (4.4) is that the ore is non-porous.

Although the feed-rate of ore to the mill (MFS) can be controlled fairly well, the variations in feed size and feed hardness upset the equilibrium in a mill significantly and are two of the main impediments to maintaining a mill at the optimum operating level (Napier-Munn et al., 1999).

Table 4.3: Feeder, mill and cyclone parameters for the *Hulbert*-model

Parameter	Description
	Feeder and Mill Parameters
α_f	Fraction fines in the ore
α_r	Fraction rock in the ore
α_P	Fractional power reduction per fractional reduction from maximum mill speed
α_{ϕ_f}	Fractional change in kW/fines produced per change in fractional filling of mill
α_{speed}	Fraction of critical mill speed
δ_{P_s}	Power-change parameter for volume fraction solids in the mill
δ_{P_v}	Power-change parameter for volume of mill filled
D_B	Density of steel balls [t/m^3]
D_S	Density of feed ore [t/m^3]
ε_{sv}	Maximum fraction of solids by volume of slurry at zero slurry flow
ϕ_b	Steel abrasion factor [kWh/t]
ϕ_f	Power needed per tonne of fines produced [kWh/t]
ϕ_r	Rock abrasion factor [kWh/t]
$\varphi_{P_{max}}$	Rheology factor for maximum mill power draw
P_{max}	Maximum mill motor power draw [kW]
v_{mill}	Mill volume [m^3]
$v_{P_{max}}$	Fraction of mill volume filled for maximum power draw
V_V	Volumetric flow per "flowing volume" driving force [h^{-1}]
χ_P	Cross-term for maximum power draw
	Cyclone Parameters
α_{su}	Parameter related to fraction solids in underflow
C_1	Constant
C_2	Constant
C_3	Constant
C_4	Constant
ε_c	Parameter related to coarse split [m^3/h]

4.2.2 Mill module

The mill module is the most crucial part of the circuit. This is where the valuable elements are liberated from the ore. The model for the mill accounts for the effect of slurry rheology and the mill power draw on the breakage of the ore.

The population volume balance of the hold-up of water (X_{mw}), solids (X_{ms}), fines (X_{mf}), rocks (X_{mr}) and balls (X_{mb}) in the mill are defined in terms of the inflow and outflow of each state:

$$\frac{d}{dt}X_{mw} = V_{mwi} - V_{mwo} \tag{4.6}$$

$$\frac{d}{dt}X_{ms} = V_{msi} - V_{mso} + RC \tag{4.7}$$

$$\frac{d}{dt}X_{mf} = V_{mfi} - V_{mfo} + FP \tag{4.8}$$

$$\frac{d}{dt}X_{mr} = V_{mri} - RC \tag{4.9}$$

$$\frac{d}{dt}X_{mb} = V_{mbi} - BC \tag{4.10}$$

where RC refers to rock consumption, BC refers to ball consumption and FP refers to fines production. These three breakage functions are described in eqs. (4.17), (4.18) and (4.19) respectively. The mill inlet flow-rates for water (V_{mwi}), solids (V_{msi}), fines (V_{mfi}), rocks (V_{mri}) and balls (V_{mbi}) are described in the equation below in terms of the feeder outflow defined in eqs. (4.1)-(4.5) and the cyclone underflow defined in eqs. (4.37), (4.40) and (4.41):

$$[V_{mwi}, V_{msi}, V_{mfi}, V_{mri}, V_{mbi}]^T = [V_{fwo} + V_{cwu}, V_{fso} + V_{csu}, V_{ffo} + V_{cfu}, V_{fro}, V_{fbo}]^T \tag{4.11}$$

The mill outlet flow-rates for water (V_{mwo}), solids (V_{mso}), fines (V_{mfo}), rocks (V_{mro}) and balls (V_{mbo}) are defined in eqs. (4.20)-(4.23).

4.2.2.1 Rheology factor

It has been shown that slurry rheology is one of the factors that affect grinding mill performance (Shi and Napier-Munn, 2002). The empirically defined rheology factor (φ) is an attempt to incorporate the effect of the fluidity and density of the slurry on the milling circuit's performance. Random close packing of hard spheres cannot exceed approximately 64% of solids by volume, whereas random loose packing gives approximately 55% of solids by volume (Song et al., 2008). This means that the slurry in the mill cannot contain less than approximately 36% water by volume. For the fully

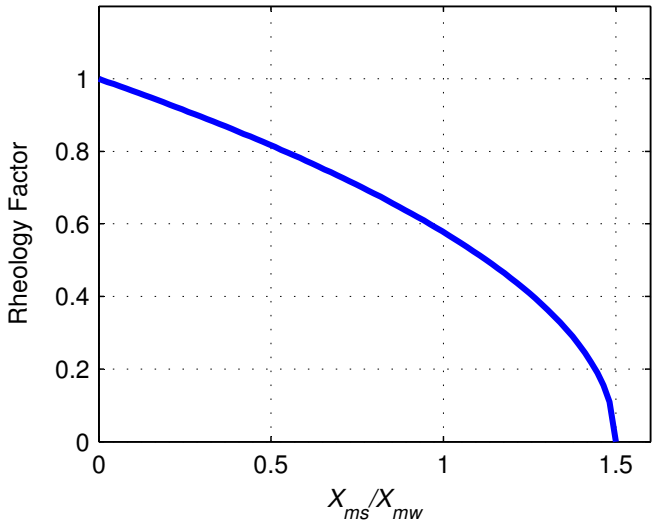

Figure 4.2: Rheology factor φ.

mixed mill the solids in the slurry are not necessarily spherical. Therefore, the non-flowing slurry is approximated to contain 40% water by volume, and the maximum fraction of solids by volume of slurry (ε_{sv}) is 0.6. The volume of water is given by X_{mw} and the total volume of the slurry is given by the sum of the volume of water and solids ($X_{mw}+X_{ms}$), which results in the relation $X_{ms}/X_{mw} = 1.5 = (1/\varepsilon_{sv}-1)^{-1}$ for a non-flowing slurry. If the slurry is purely water, then $X_{ms}/X_{mw} = 0$. The function to describe the rheology factor (φ) is chosen to go from 1 for 100% water, to approximately 0.55 when the volume of solids (X_{ms}) is equal to the volume of water (X_{mw}), and to 0 for non-flowing mud at around 40% water by volume. Equation (4.12) achieves these three criteria and is plotted in Fig. 4.2.

$$\varphi = \left\{ \max \left[0, 1 - \left(\left(\frac{1}{\varepsilon_{sv}} \right) - 1 \right) \frac{X_{ms}}{X_{mw}} \right] \right\}^{0.5} \tag{4.12}$$

The rheology factor (φ) is similar in concept to viscosity. To relate it to viscosity by a model is not particularly productive. The first problem is that the slurry is not a Newtonian fluid, so its stress-strain relationship is not defined by only one viscosity parameter. Even if the viscosity is modelled perfectly, assumptions and complex modelling would be necessary of how various amounts of balls, rocks, coarse material and slurry move in a mill. The motion of the charge in the mill is in turn a function of flow-rates, viscosities, the shape of lifters, the shape of the discharge grate, etc. Instead of using an intermediate variable (viscosity) that creates more questions than answers, the easily calculated rheology factor in eq. (4.12) characterises the fluidity of slurry. This rheology factor (φ)

of the slurry can be used as a tool to model the effect of slurry water content on for example power draw and abrasion rates that depend on the thickness of the slurry.

4.2.2.2 Mill Power Draw

There are a number of mill power draw models that are valuable for the design and scale-up of grinding mills, such as the models found in Apelt et al. (2001), Austin (1990) and Morrell (2004). These models model mill power draw by means of a multi-parameter non-symmetrical curve as a function of the mass of material in the mill to make the power drop off suddenly as the mill becomes overfilled. However, the quick decline in mill power as the mill becomes overfilled is unlikely to only be due to the mass of the load. It is also due to a complicated effect of rheology that depends on water content and solids build-up within particular size classes. The complex interaction between water and solids concentrations and rheology and load cascading/sliding/tumbling still has to be solved comprehensively.

The mill power draw model presented here is made to rely on the lowest number of dependent variables that can be used to produce the required characteristics of the response. The power draw of the mill will be low for a very watery load and also for a load with low water content. In the first instance, the load forms a puddle at the bottom of the mill, whereas for low water content the load forms a ball of mud that rolls with little absorption of power. Somewhere in the middle the power reaches a maximum when the water content makes the load ride up the side of the mill to the maximum extent. Thus, the mill power draw can be modelled to depend on only two variables: the rheology factor of the slurry and the total charge inside the mill at which the maximum mill power draw occurs. For control purposes, accuracy far away from the maximum is not important, since the functional form of the mill power draw ensures that the power drops significantly and increasingly on both sides.

The mill power draw for the *Hulbert*-model is defined as:

$$P_{mill} = P_{max}\{1 - \delta_{Pv}Z_x^2 - 2\chi_P\delta_{Pv}\delta_{Ps}Z_xZ_r - \delta_{Ps}Z_r^2\} \cdot (\alpha_{speed})^{\alpha_P} \tag{4.13}$$

where P_{max} (kW) is the maximum mill motor power draw, δ_{Pv} and δ_{Ps} are the power change parameters for volume of the mill filled and the volume fraction of solids in the mill respectively, χ_P is the cross-term for maximum power draw, α_{speed} is the fraction of critical mill speed and α_P is the fractional change in kW/fines produced per change in fractional filling of the mill. The effect of the

total charge on mill power (Z_x) is given by the empirically defined equation:

$$Z_x = \frac{LOAD}{v_{mill} \cdot v_{P_{max}}} - 1 \tag{4.14}$$

where v_{mill} (m^3) is the volume of the mill, $v_{P_{max}}$ is the fraction of the mill filled for maximum power draw and $LOAD$ describes the mill charge volume in terms of the volumetric states in the mill:

$$LOAD = X_{mw} + X_{mr} + X_{ms} + X_{mb} \tag{4.15}$$

The effect of the slurry rheology on mill power (Z_r) is given by the empirically defined equation:

$$Z_r = \frac{\varphi}{\varphi_{P_{max}}} - 1 \tag{4.16}$$

where $\varphi_{P_{max}}$ is the rheology factor for maximum mill power draw. The significance of the parameters in eqs. (4.13)-(4.16) are discussed in following paragraphs.

As can be seen from eq. (4.13), the maximum mill power draw (P_{max}) is reached if the effect of slurry rheology (Z_r) and the effect of the charge in the mill (Z_x) on the mill power draw is zero, i.e. Z_r and Z_x are equal to zero. Two parameters are defined to achieve this: the rheology factor for maximum mill power draw $\varphi_{P_{max}}$ and the mill filling for maximum mill power draw $v_{P_{max}}$. Therefore, when $\frac{LOAD}{v_{mill}} = v_{P_{max}}$ and $\varphi = \varphi_{P_{max}}$, both Z_x and Z_r are zero.

The drop-off rate of the mill power draw (P_{mill}) is modelled as parabolic, with drop-off parameters for the effect of slurry rheology (Z_r) and the effect of the mill charge (Z_x) on the mill power draw. Thus, δ_{Ps} is the power-change parameter for the fraction of solids in the mill and δ_{Pv} is the power-change parameter for the total charge in the mill. The values for these two parameters depend on the dynamic response of the mill power draw to changes in the mill environment. By default they are set to unity, which results in a fast decrease/increase of the mill power draw to changes in the mill environment. If a slower response is needed, the values can be made lower. In general, sampling campaign data, good knowledge of the plant and simplifying assumptions are necessary to choose the parameter values with any accuracy.

The term $\chi_P \delta_{Pv} \delta_{Ps} Z_x Z_r$ in eq. (4.13) models the dependence of the maximum power draw with respect to one of the variables (effect of rheology Z_r or effect of the charge Z_x) on the value of the other. The parameter χ_P determines the magnitude of this cross term for maximum power draw. It is unsure if this parameter should be positive or negative. If there is no mill power draw data available to support the fit of this parameter, the value for χ_P is chosen as zero.

Lastly, the mill power draw in eq. (4.13) is proportional to the speed at which the mill runs. The parameter introduced here is the fraction of the critical mill speed α_{speed}. This parameter is raised to the power α_P, the fractional power reduction per fractional reduction from critical mill speed. Unless survey data are available to fit this parameter, the value of α_P is chosen as unity.

In Powell et al. (2009, 2011) grindcurves are developed which relate mill filling to mill power draw. These studies give an indication of how a sampling campaign can be conducted to obtain the parameters mentioned above. An example of the effect that changes in the mill environment and the mill speed has on the power draw and the performance of an industrial grinding mill circuit can be seen in Viklund et al. (2006).

4.2.2.3 Breakage functions

As the ore grinds in the mill, it results in the consumption of rocks and balls over time, as well as the production of fines. The definition for rock consumption is:

$$RC = \frac{P_{mill} \cdot \varphi}{D_S \phi_r} \left(\frac{X_{mr}}{X_{mr} + X_{ms}} \right) \tag{4.17}$$

where ϕ_r (kWh/t) describes rock abrasion inside the mill, i.e. the rate at which rocks are consumed inside the mill. The mass of the ore hold-up inside the mill is given by $D_S \cdot (X_{mr} + X_{ms})$. The rheology factor ($\varphi$) is included in the rock consumption function in eq. (4.17) to model the effect of the density of the slurry on breakage. The abrasion rate of rocks is at its maximum in a watery grinding paste, represented by the rheology factor near 0.8. This is a practical finding - milling with more water gives a higher throughput with faster rock abrasion and a coarser grind. As the slurry becomes thicker, it cushions the interaction between the grinding media, and throughput drops, rock breakage rates decrease and the product becomes finer (Napier-Munn et al., 1999).

Ball consumption is defined as:

$$BC = \frac{P_{mill} \cdot \varphi}{\phi_b} \left(\frac{X_{mb}}{D_S \cdot (X_{mr} + X_{ms}) + D_B \cdot X_{mb}} \right) \tag{4.18}$$

where ϕ_b (kWh/t) is the steel abrasion factor, i.e. the rate at which balls are consumed within the mill. The mass of ore and balls in the mill is given by $D_S \cdot (X_{mr} + X_{ms}) + D_B \cdot X_{mb}$. The ball consumption equation follows the same reasoning as for rock consumption defined in eq. (4.17).

The production of fines in the mill is defined as:

$$FP = \frac{P_{mill}}{D_S \cdot \left\{ \phi_f \cdot \left[1 + \alpha_{\phi_f} \cdot \left(\frac{LOAD}{v_{mill}} - v_{P_{max}} \right) \right] \right\}} \tag{4.19}$$

where ϕ_f (kWh/t) is the power needed per tonne of fines produced and α_{ϕ_f} is the fractional change in power per fines produced per change in fractional filling of the mill. The fines produced from rocks are not distinguished from fines produced from the coarse ore. Therefore the fines production from rocks and coarse ore are lumped. If the mill operates at the optimal load volume for maximum mill power draw, eq. (4.19) reduces to $\frac{P_{mill}}{D_S \phi_f}$. The approximation of a rate of fines production per power input is considered an acceptable assumption for the reasons stated below. With more power, ore tends to break or wear away more even though only a small portion of the power goes into extra surface creation and most goes into heating. If one assumes breakage proportional to power, the error might be 5-15%. If one models breakage by the single particle breakage tests found in Napier-Munn et al. (1999), the results can be difficult to correct to 5-15% and the models do not necessarily relate power to breakage. The easily measurable power might be discarded even though it contains rich information about milling conditions. It is common to use the empirical connection between breakage rates and power, because it is easier to correlate with plant data and does not require extensive test work.

The rate of fines production per power input is not quite constant - it increases slightly when the mill filling is lower than the filling at which maximum power is drawn. For this reason the factor $\left[1 + \alpha_{\phi_f} \cdot \left(\frac{LOAD}{v_{mill}} - v_{P_{max}} \right) \right]$ is included in eq. (4.19), where α_{ϕ_f} accounts for the fractional change in power per fines produced per change in fractional filling of the mill. In other words, it is the slope of the power needed for a tonne of fines produced per volume of the mill filled. Unless survey data are available to determine the slope of the curve, a conservative value of α_{ϕ_f} is chosen as 0.01.

The rheology factor (φ) influences the breakage rate of fines indirectly by changing the modelled power draw (P_{mill}), which is assumed to be proportional to the breakage rate of fines. The power draw is a good intermediate variable since a mill running at relatively high power draw is invariably running at relatively high fines production rates. At present, there are no data or rationale to assume that the conversion of power draw (which is a function of fluidity) to fines production improves with higher fluidity or lower fluidity. For this reason the rheology factor (φ) is not included in eq. (4.19).

4.2.2.4 Discharge flow-rates

The discharge flow-rates of water (V_{mwo}), solids (V_{mso}), fines (V_{mfo}), rocks (V_{mro}) and balls (V_{mbo}) through the end-discharge screen are defined as:

$$V_{mwo} = V_V \cdot \varphi \cdot X_{mw} \cdot \left(\frac{X_{mw}}{X_{ms} + X_{mw}} \right) \tag{4.20}$$

$$V_{mso} = V_V \cdot \varphi \cdot X_{mw} \cdot \left(\frac{X_{ms}}{X_{ms} + X_{mw}} \right) \tag{4.21}$$

$$V_{mfo} = V_V \cdot \varphi \cdot X_{mw} \cdot \left(\frac{X_{mf}}{X_{ms} + X_{mw}} \right) \tag{4.22}$$

$$V_{mro} = V_{mbo} = 0 \tag{4.23}$$

where V_V is the volumetric flow per "flowing volume" driving force. The driving force is the pressure applied to the slurry to discharge from the mill. The hold-up of water (X_{mw}) and solids (X_{ms}) contained in the mill are the two main contributors to the driving force. Since the rheology factor (φ) already considers the effect of the volume of solids (X_{ms}), only the volume of water (X_{mw}) is multiplied with parameter V_V. Still, it is possible to multiply the sum of the volume of water and solids ($X_{mw} + X_{ms}$) instead of only the volume of water (X_{mw}) with the driving force in eqs. (4.20)-(4.22) above. The rheology factor (φ) is included to model the case of flow of the slurry through the discharge grate. The last term in brackets in eq. (4.20)-(4.22) provides the fraction of the relevant state of the volume of material that can be discharged from the mill. The flow-rate for rocks and balls (V_{mro} and V_{mbo}) out of the mill is zero since it is assumed rocks and balls are too large to discharge from the mill through the screen.

4.2.3 Mixed-sump module

For this module the assumption is made that the constituents inside the sump are fully mixed. This assumption is only valid if the sump is operated at the correct level, i.e. if the sump level is too low, air-entrainment could ensue; if the sump level is too high, a pool of stagnant liquid could form. Also, this assumption will only affect the dynamic response and not the steady-state response of the sump (Hinde and King, 1978).

The only constituents or states found in this module are water, solids and fines. The population volume balance of the hold-up of water (X_{sw}), solids (X_{ss}) and fines (X_{sf}) in the sump are defined as:

$$\frac{d}{dt} X_{sw} = V_{swi} - V_{swo} + SFW \tag{4.24}$$

$$\frac{d}{dt}X_{ss} = V_{ssi} - V_{sso} \tag{4.25}$$

$$\frac{d}{dt}X_{sf} = V_{sfi} - V_{sfo} \tag{4.26}$$

where V_{swi}, V_{ssi} and V_{sfi} represent the flow-rate of water, solids and fines into the sump respectively, and V_{swo}, V_{sso} and V_{sfo} represent the flow-rate of water, solids and fines out of the sump respectively. Equation (4.24) includes the flow-rate of water added to the slurry in the sump (SFW) to manipulate the density of the slurry feed to the cyclone. This density has a significant impact on the performance of the cyclone. The cyclone feed density is defined as $CFD = \frac{X_{sw}+D_s \cdot X_{ss}}{X_{sw}+X_{ss}}$ where the numerator gives the mass and the denominator the volume of the material that can be discharged from the sump.

The sump inflow of water (V_{swi}), solids (V_{ssi}) and fines (V_{sfi}) can be described in terms of the mill outflow defined in eqs. (4.20)-(4.22):

$$[V_{swi}, V_{ssi}, V_{sfi}]^T = [V_{mwo}, V_{mso}, V_{mfo}]^T \tag{4.27}$$

The sump discharge flow-rates of water (V_{swo}), solids (V_{swo}) and fines (V_{sfo}) are defined as:

$$V_{swo} = CFF \cdot \left(\frac{X_{sw}}{SVOL}\right) \tag{4.28}$$

$$V_{sso} = CFF \cdot \left(\frac{X_{ss}}{SVOL}\right) \tag{4.29}$$

$$V_{sfo} = CFF \cdot \left(\frac{X_{sf}}{SVOL}\right) \tag{4.30}$$

where CFF is the cyclone feed flow-rate and $SVOL$ is the volume of slurry in the sump:

$$SVOL = X_{sw} + X_{ss} \tag{4.31}$$

The cyclone feed flow-rate (CFF) is equal to the sum of V_{swo} and V_{sso}. The flow-rates defined in eqs. (4.28)-(4.30) are determined by multiplying the cyclone feed flow-rate (CFF) with the fraction of the volume which a state occupies within the total volume of the slurry inside of the sump.

4.2.4 Hydrocyclone module

Although the hydrocyclone model was briefly presented in Coetzee et al. (2010), a detailed description of the model equations is presented here. Because the dynamics of the hydrocyclone are much faster than the rest of the circuit, the hydrocyclone is described by a set of algebraic equations.

In the Plitt equation the corrected classification-size (d_{50_c}) is proportional to $\frac{exp(6.3F_i)}{(CFF)^{0.45}}$, where F_i is the fraction of solids in the total inflow volume and CFF is the cyclone feed flow-rate (Nageswararao et al., 2004). Thus, the definition of F_i is:

$$F_i = \frac{V_{csi}}{CFF} \tag{4.32}$$

where V_{csi} is the volumetric flow-rate of solids into the cyclone.

If the classification-size (d_{50_c}) increases, less coarse ore in the inflow to the cyclone (V_{cci}) will report to the underflow of the cyclone (V_{ccu}). It should be remembered that solids are defined as the sum of coarse ore and fine ore. Because the flow of coarse ore to the underflow (V_{ccu}) will constrain the flow of water to the underflow (V_{cwu}) and fines to the underflow (V_{cfu}), the actual split of coarse ore in the inflow to the cyclone (V_{cci}) needs to be determined before the split of fines that enter the cyclone (V_{cfi}) can be determined. Thus, the flow-rate of coarse ore at the underflow (V_{ccu}) is considered to be a function of:

- cyclone coarse ore inflow V_{cci}, as the primary dependency,
- cyclone feed flow-rate CFF, which determines the main centrifugal driving force in terms of inlet velocity,
- fraction of solids in the total inflow volume F_i, which relates to the degree of constrained rather than free particle movement, and
- the fraction of fines in feed solids P_i, which relates to viscosity and also indicates how much nearly-fine material is in the coarse fraction.

Accurate modelling of the low-flow conditions is not considered in the derivation of the model for the coarse split. Therefore, a functional form is used that gives a split between coarse ore underflow and inflow of $V_{ccu} = AV_{cci}$ as the cyclone feed flow-rate (CFF) becomes very small. The constant A can be used to shape the higher-flow part of the function instead of making the low-flow part accurate. From the Plitt equation, an increase in cyclone feed flow-rate (CFF) results in a reduction of the classification-size (d_{50_c}). Therefore, as the cyclone feed flow-rate (CFF) increases, the flow of coarse ore at the underflow (V_{ccu}) should increase asymptotically to the flow of coarse ore into the cyclone (V_{cci}). Thus, the sensitivity of the coarse material split to the total cyclone feed flow-rate is given

by:

$$\left(\frac{V_{ccu}}{V_{cci}}\right)_1 = 1 - C_1 \cdot \exp\left(-CFF/\varepsilon_c\right) \tag{4.33}$$

where parameter C_1 relates to the split at low-flows when the centrifugal force is relatively small and the cyclone acts like a pipe T-piece, and parameter ε_c (m^3/h) defines how quickly the flow of coarse material to the overflow drops towards zero exponentially as a result of increasing centrifugal forces when the feed flow increases to high values. As seen from experimentation in Hulbert (2005), a prudent value for C_1 is 0.6. Equation (4.33) is plotted in Fig. 4.3a with parameter values as determined in Section 4.3.

The upper limit of the packing fraction of solid particles is approximately 0.6. Thus, the upper limit of the fraction solids in the feed (F_i) is 60%. As can be seen from the Plitt equation, the amount of coarse ore in the inflow (V_{cci}) that passes to the underflow (V_{ccu}) will decrease when the fraction solids in the feed (F_i) increases. This places a constraint on the coarse ore in the underflow (V_{ccu}) in terms of the fraction solids in the feed (F_i). Therefore:

$$\left(\frac{V_{ccu}}{V_{cci}}\right)_2 = 1 - \left(F_i/C_2\right)^{C_3} \tag{4.34}$$

where C_2 is a constant which normalises the fraction solids in the feed (F_i) according to the upper limit for the packing fraction of solid particles and C_3 determines the sharpness of the curve. Equation (4.34) is plotted in Fig. 4.3b with parameter values as determined in Section 4.3. This equation is unity when the fraction solids in the feed (F_i) is low. As the fraction solids in the feed (F_i) approaches that of thick mud (between 0.6 and 0.7), the relative movement of coarse material decreases towards zero. When this happens, the underflow is blocked and all the slurry goes to the overflow. Parameter C_3 defines the rate at which the equation above plunges towards zero. If C_3 is unity, the equation would be linear and not appropriate.

The last variable to consider for the coarse split model is the fraction fines in the feed solids (P_i). In terms of the inflow of fines (V_{cfi}) and solids (V_{csi}), P_i is defined as:

$$P_i = \frac{V_{cfi}}{V_{csi}} \tag{4.35}$$

If the fraction fines in the feed solids (P_i) is small, it indicates that the material is very coarse. Alternatively, if P_i is very large, it indicates the presence of more finer material in the coarse fraction. Therefore:

$$\left(\frac{V_{ccu}}{V_{cci}}\right)_3 = 1 - P_i^{C_4} \tag{4.36}$$

where C_4 is a constant which defines how quickly the function decreases towards zero. Equation (4.36) is plotted in Fig. 4.3c with parameter and flow-rate values as determined in Section 4.3. If the fraction of fines in the feed solids (P_i) is small, it indicates that the coarse material is very coarse. Alternatively, if the fraction of fines in the feed solids (P_i) is large, it indicates that there is more near-sized finer material in the coarse fraction. The effect starts at unity for low fines and decreases towards zero when almost all the solids in the feed material (V_{csi}) is fine. In this case, the small amount of coarse material is close to being fine and the viscous effects of a large volume of fines would hinder the settling movement of the coarse material.

The final underflow from the hydrocyclone to the mill for the coarse solids is defined as the multiplicative effect of the sensitivity of the coarse split to the total cyclone feed flow-rate (eq. (4.33)), of the sensitivity of the coarse split to the volume fraction of solids in the cyclone feed flow-rate (eq. (4.34)) and of the sensitivity of the coarse split to the fraction of fines in the solids feed flow-rate (eq. (4.36)):

$$\frac{V_{ccu}}{V_{cci}} = \left(\frac{V_{ccu}}{V_{cci}}\right)_1 \left(\frac{V_{ccu}}{V_{cci}}\right)_2 \left(\frac{V_{ccu}}{V_{cci}}\right)_3 = \left(1 - C_1 e^{\left(\frac{-CFF}{\varepsilon_c}\right)}\right) \left(1 - \left(\frac{F_i}{C_2}\right)^{C_3}\right) \left(1 - P_i^{C_4}\right) \tag{4.37}$$

To determine the amount of water and fines that accompany the coarse material to the underflow, the fraction of solids in the underflow volume (F_u) must be determined. This is modelled as a function of the fraction of solids in the inflow (F_i) as the primary dependency at low values of the coarse ore underflow (V_{ccu}), and the coarse ore underflow (V_{ccu}) as the primary dependency at high values of the coarse ore underflow (V_{ccu}). If V_{ccu} increases, it is only logical that the fraction of solids in the underflow volume (F_u) should also increase. Again, the maximum packing fraction is approximated as 0.6, which places an upper limit on F_u. Therefore:

$$F_u = 0.6 - (0.6 - F_i) \cdot e^{(-V_{ccu}/(\alpha_{su}\varepsilon_c))} \tag{4.38}$$

where α_{su} relates to the fraction of solids in the underflow. Equation (4.38) is shown in Fig. 4.3d with parameter values as determined in Section 4.3. At around zero coarse ore underflow (V_{ccu}), the underflow consists primarily of feed material and $F_u \approx F_i$. As the flow of coarse material in underflow (V_{ccu}) increases, it increasingly squeezes the fines (V_{cfu}) and water (V_{cwu}) out of the underflow, asymptotically reaching the thickest possible mud at a solids fraction of about 0.6.

The fraction of solids in the underflow can also be written in terms of the underflow of fines (V_{cfu}),

coarse ore (V_{ccu}) and water (V_{cwu}):

$$F_u = \frac{V_{cfu} + V_{ccu}}{V_{cwu} + V_{cfu} + V_{ccu}} \tag{4.39}$$

The ratio of fines to water in the overflow, underflow and cyclone feed is assumed to be the same, as the fines are considered to be fine enough not to be influenced by the centrifugal forces. Thus: $V_{cwu}/V_{cwi} = V_{cfu}/V_{cfi}$. With these ratios and eq. (4.39), the underflow of water (V_{cwu}) and fines (V_{cfu}) can be determined:

$$V_{cwu} = \frac{V_{cwi}\,(V_{ccu} - F_u V_{ccu})}{(F_u V_{cwi} + F_u V_{cfi} - V_{cfi})} \tag{4.40}$$

$$V_{cfu} = \frac{V_{cfi}\,(V_{ccu} - F_u V_{ccu})}{(F_u V_{cwi} + F_u V_{cfi} - V_{cfi})} \tag{4.41}$$

The cyclone inflow for water (V_{cwi}), coarse ore (V_{cci}), solids (V_{csi}) and fines (V_{cfi}) can be described in terms of the sump outflows defined in eqs. (4.28)-(4.30), as shown below.

$$[V_{cwi}, V_{cci}, V_{csi}, V_{cfi}]^T = [V_{swo}, V_{sso} - V_{sfo}, V_{sso}, V_{sfo}]^T \tag{4.42}$$

The product particle size (PSE) at the cyclone overflow is defined as the fraction of fines present in the total output flow of the cyclone:

$$PSE = \frac{V_{cfo}}{V_{cco} + V_{cfo}} = \frac{V_{cfi} - V_{cfu}}{V_{cci} - V_{ccu} + V_{cfo}} \tag{4.43}$$

where the V_{cfo} is the overflow of fines and V_{cco} is the overflow of coarse ore.

4.3 PARAMETER ESTIMATION

4.3.1 Data for model fit

The data of five sampling campaigns on an existing single-stage grinding mill circuit at steady-state were provided by an industrial plant. The survey data gave the cumulative distribution of ore in 25 size classes for the inlet and outlet flows of each unit in the circuit. The key variables measured during the five surveys are shown in Table 4.4.

Survey 3 presented the best results in terms of throughput, grind size, and energy efficiency. Therefore, the data from this survey are used to fit the parameters of the *Hulbert*-model. The other four surveys are used for the validation of the model.

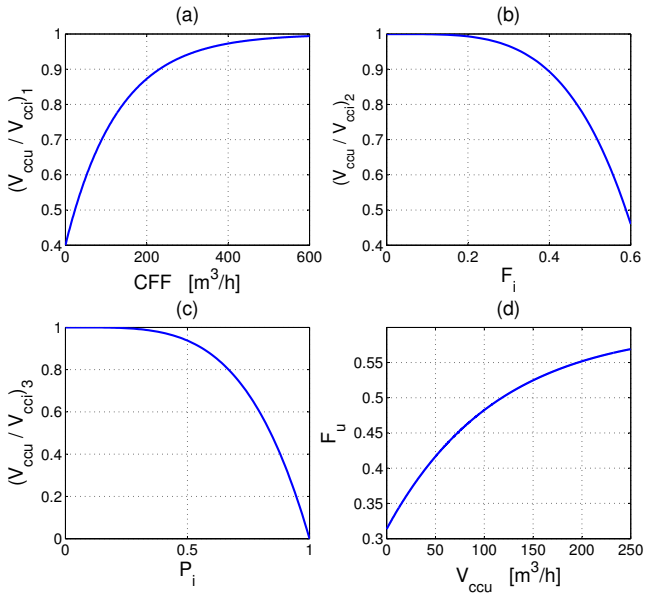

Figure 4.3: (a) Eq. (4.33): sensitivity of the coarse split to cyclone feed flow CFF. (b) Eq. (4.34): sensitivity of the coarse split to fraction solids in the cyclone feed flow F_i. (c) Eq. (4.36): sensitivity of the coarse split to fraction fines the feed solids P_i. (d) Eq. (4.38): sensitivity of fraction of solids in the underflow volume to the coarse ore underflow V_{ccu}.

During the sampling campaign, no attempt was made to estimate the ore, water and ball charge from crash stops and grind-out tests for each of the surveys. The only information received from the plant was that the mill was operated with a total charge filling of about 34% of mill volume. Therefore, the estimation for the total charge within the mill ($LOAD$) in eq. (4.15) is 20.1 m^3 for the third survey, given that the total mill volume (v_{mill}) is 59.12 m^3.

To determine the volume of slurry in the sump ($SVOL$) in eq. (4.31), it is known that the cross section of the sump is 1.1 m by 3.2 m, the height to the centre line of the pump is 0.7 m and the controlled slurry level above the pump inlet is 1.0 m. Therefore, $SVOL$ is estimated as 5.99 m^3.

It was stated by the plant that the mill was run at a constant ball charge of approximately 24% of the mill volume, which gives an estimate for the weight of the balls at $w_b = 66.8$ t. Also, the same type of ore is used for all the surveys. Thus, it is assumed that the total mass of balls within the mill and the size distribution of the ore feed remain constant for all five surveys.

The sampling campaigns provided only steady-state values. No dynamic data were available for parameter estimation.

Table 4.4: Survey data

Survey:	1	2	3	4	5
MIW (m^3/h)	4.71	4.45	4.64	3.66	4.22
MFS (t/h)	66.9	61.7	65.2	46.7	57.2
MFB (t/h)	6.43	5.38	5.69	6.77	6.58
SFW (m^3/h)	67.1	67.1	140.5	69.3	70.4
CFF (m^3/h)	267	224	374	294	305
PSE (Fraction)	0.60	0.55	0.67	0.68	0.58
P_{mill} (kW)	1142	1120	1183	1093	1071
Circ. Load Ratio	3.6	3.2	4.7	5.9	4.9
Specific Energy	17.1	18.2	18.1	23.4	18.7
kWh/t -75μm (ϕ_f)	31.5	36.9	29.6	37.6	35.7
Constants					
Ore Density (t/m^3)	3.2	Mill volume (m^3)			59.12
Ball Density (t/m^3)	7.85	Crit. mill speed			0.712

4.3.2 Hulbert-model parameter estimation procedure

The final estimated parameter values for the plant using the data of survey 3 are shown in Table 4.5. The procedure to determine the parameters relevant to each module is discussed below.

Before the model fit can start, it is necessary to define the passing sizes that the states of the *Hulbert*-model represent. The states are described in Table 4.6 in terms of the ore sizes and constituent they represent. The state X_{mr} represents the volume of ore in the mill above the discharge grate passing size. For the plant used to fit the model, the discharge grate allowed ore smaller than 22.4 mm to pass to the sump. The states X_{ms} and X_{ss} represent the volume of ore below 22.4 mm in the mill and sump respectively, i.e. the volume of solids in the mill and sump. The product specification size was 75 μm, which means that the states X_{mf} and X_{sf} are the volume of ore passing 75 μm in the mill and sump respectively, i.e. the volume of fines in the mill and sump. The states X_{mw} and X_{sw} are the volume of water in the mill and sump respectively, and X_{mb} is the volume of balls in the mill.

The cumulative distribution of ore for survey 3 passing each of the 25 size classes is plotted in Fig.

Table 4.5: Estimated parameter values and initial states

Parm	Value	Units	Parm	Value	Units
Mill and Feeder Parameters					
α_f	0.055	-	ϕ_b	90.0	kWh/t
α_r	0.465	-	ϕ_f	29.6	kWh/t
α_P	1	-	ϕ_r	6.03	kWh/t
α_{speed}	0.712	-	$\varphi_{P_{max}}$	0.57	-
α_{ϕ_f}	0.01	-	P_{max}	1662	kW
δ_{P_s}	0.5	-	v_{mill}	59.12	m^3
δ_{P_v}	0.5	-	$v_{P_{max}}$	0.34	-
D_B	7.85	t/m^3	V_V	84.0	-
D_S	3.2	t/m^3	χ_P	0	-
ε_{sv}	0.6	-			
Cyclone Parameters					
α_{su}	0.87	-	C_3	4	-
C_1	0.6	-	C_4	4	-
C_2	0.7	-	ε_c	129	m^3/h
States					
X_{mb}	8.51	m^3	X_{mw}	4.85	m^3
X_{mf}	1.09	m^3	X_{sf}	0.42	m^3
X_{mr}	1.82	m^3	X_{ss}	1.88	m^3
X_{ms}	4.90	m^3	X_{sw}	4.11	m^3

4.4. From this figure, the cumulative percentages of ore passing 22.4 mm and 75 μm are listed in Table 4.7. The table also shows the flow-rates of the total ore and water at the inlet and outlet of each unit. The data in Table 4.7 is used to estimate the parameters in the *Hulbert*-model.

4.3.2.1 Feeder

The feeder module has only two parameters to fit, α_r and α_f, where α_r is the fraction of ore in the feed that is larger than the aperture size of the discharge grate of the mill and α_f is the fraction of ore in the feed that is smaller than the final product specification size. The values for these two parameters

Table 4.6: Description of the states within the mill and sump

Constituents	Mill States	Sump States
Ore $>$ 22.4 mm	X_{mr}	
Ore $\leq$ 22.4 mm	X_{ms}	X_{ss}
Ore $\leq$ 75 μm	X_{mf}	X_{sf}
Water	X_{mw}	X_{sw}
Balls	X_{mb}	

Table 4.7: Flow-rates of Survey 3 (Percentages are the cumulative percentage of ore passing size x_i)

	Feeder	Mill	
Size x_i	New Feed	Inlet	Outlet
22.4 mm	53.5%	91.9%	100%
0.075 mm	5.51%	11.5%	22.2%
Total ore (t/h)	65.2	374.7	374.7
Water (m^3/h)	4.64	115.9	115.9
	Sump	Cyclone	
Size x_i	Dilution	UF	OF
22.4 mm	-	100%	100%
0.075 mm	-	12.8%	66.8%
Total ore (t/h)	-	309.5	65.2
Water (m^3/h)	140.5	111.3	145.1

can be obtained from the second column in Table 4.7: $\alpha_r = 0.465$ and $\alpha_f = 0.055$.

4.3.2.2 Mill

The first step in fitting the mill module parameters is to define the mill power draw parameters in eq. (4.13). It is assumed that the cross-term for maximum power (χ_P) is zero and the fraction power reduction per fractional reduction from maximum mill speed (α_P) is unity since no data were available to fit these parameters. The plant provided time-series plots of the mill power draw, which gave an indication of the rate and magnitude of change in the mill power draw. From the plots provided by

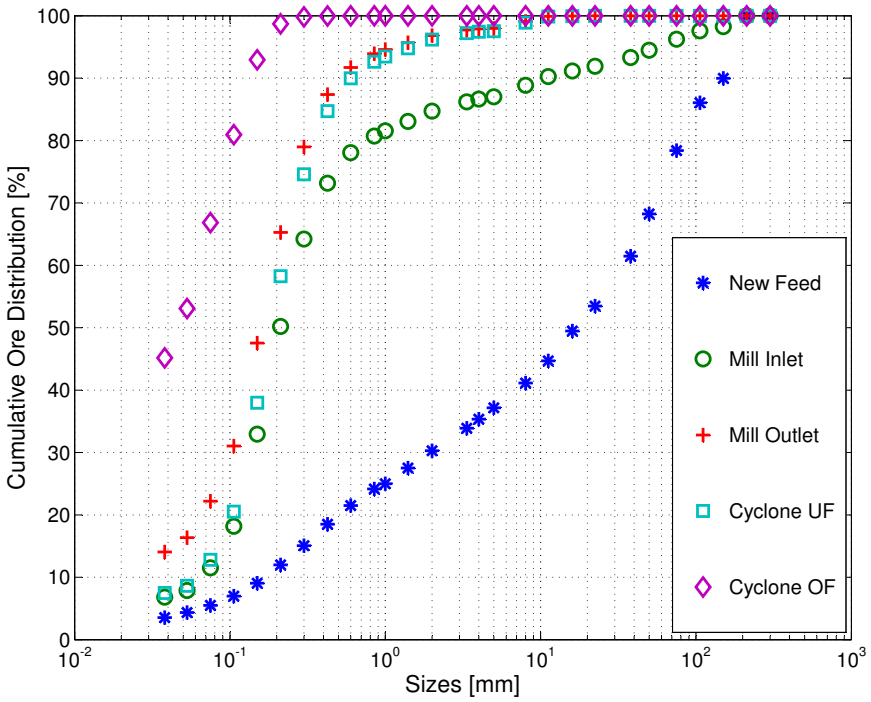

Figure 4.4: The cumulative ore distribution for survey 3 of the feeder outlet, the mill inlet and outlet, and the cyclone underflow (UF) and overflow (OF).

the plant, the power-change parameters for fraction solids (δ_{Ps}) and charge volume (δ_{Pv}) in the mill were set equal to 0.5.

Because the third survey provided the best results, and no additional information was available to determine the peak of the power-load curve, it is assumed that the data of the third survey represent the optimal operating condition of the grinding mill circuit. It is assumed that both the effect of the mill load (Z_x) and the effect of the slurry rheology (Z_r) on the mill power draw (P_{mill}) are zero and therefore $P_{mill} = P_{max}\left(\alpha_{speed}\right)^{\alpha_P}$. Given the critical mill speed (α_{speed}) and the mill power draw (P_{mill}) from survey data, it means that the maximum mill power draw is $P_{max} = 1183/0.712 = 1662$ kW.

If $Z_x = 0$, there is a constraint on the sum of the states in the mill:

$$X_{mw} + X_{mr} + X_{ms} + X_{mb} = v_{mill} v_{P_{max}} = LOAD \tag{4.44}$$

Because both the volume of the charge in the mill ($LOAD$) and the mill volume (v_{mill}) are known, it means that $v_{P_{max}} = 20.1/59.12 = 0.34$.

If $Z_r = 0$, the rheology factor for maximum mill power ($\varphi_{P_{max}}$) is equal to φ in eq. (4.12). It is not

necessary to know the values of the volume of water (X_{mw}) and volume of solids (X_{ms}) in the mill to determine the rheology factor (φ), as only the ratio between the two is required. This ratio can be determined by dividing eq. (4.21) by (4.20):

$$\frac{V_{mso}}{V_{mwo}} = \frac{X_{ms}}{X_{mw}} \tag{4.45}$$

Thus, given that the maximum fraction of solids by volume of slurry (ε_{sv}) is fixed at 0.6:

$$\varphi_{P_{max}} = \left[1 - \left(\frac{1}{0.6} - 1\right)\frac{V_{mso}}{V_{mwo}}\right]^{0.5} = 0.572 \tag{4.46}$$

For the breakage functions, the abrasion rate of balls (ϕ_b) is specific to the type of steel used in the mill and is generally 90 kWh/t. The power needed per tonne of fines produced (ϕ_f) is provided by the survey data as 29.6 kWh/t. Because the ball mass (w_b) within the mill is known, the volume of balls in the mill is $X_{mb} = \frac{w_b}{D_B} = 8.51$ m^3.

There are six remaining unknown quantities within the mill: the abrasion rate of rocks (ϕ_r), the volumetric flow driving force (V_V) and the hold-up of water (X_{mw}), solids (X_{ms}), fines (X_{mf}) and rocks (X_{mr}) within the mill. The six equations used to calculate these unknowns are eqs. (4.9), (4.20), (4.21), (4.22), (4.44) and (4.45). Because the survey is conducted at steady state, the left-hand side of eq. (4.9) is equal to zero. The non-linear minimization function *fmincon* with the *Interior-Point* algorithm in the Optimisation Toolbox[1] of MATLAB was used to find the solution to the following equation:

$$\begin{aligned} 0 = &\left[V_{fro} - \frac{P_{mill}\varphi_{P_{max}}}{\phi_r D_S}\left(\frac{X_{mr}}{X_{mr}+X_{ms}}\right)\right]^2 + \left[V_{mwo} - \frac{V_V \varphi_{P_{max}} X_{mw}^2}{X_{mw}+X_{ms}}\right]^2 + \left[V_{mso} - \frac{V_V \varphi_{P_{max}} X_{mw} X_{ms}}{X_{mw}+X_{ms}}\right]^2 \\ &+ \left[V_{mfo} - \frac{V_V \varphi_{P_{max}} X_{mw} X_{mf}}{X_{mw}+X_{ms}}\right]^2 + \left[LOAD - (X_{mw}+X_{ms}+X_{mr}+X_{mb})\right]^2 + \left[X_{ms} - \frac{X_{mw} V_{mso}}{V_{mwo}}\right]^2 \end{aligned} \tag{4.47}$$

The constraints for *fmincon* were chosen in light of the information provided by Table 4.7. Since the volume of the mill filled is $LOAD = 20.1$ m^3 and the volume of balls is $X_{mb} = 8.51$ m^3, there remains 11.6 m^3 to divide between the volume of solids (X_{ms}), rocks (X_{mr}) and water (X_{mw}) in the mill. Because the volumetric flow-rates of solids (V_{mso}) and water (V_{mwo}) out of the mill are almost equal according to Table 4.7, the volume of solids (X_{ms}) and water (X_{mw}) in the mill should be approximately equal according to eq. (4.45). Solids are the sum of fines and coarse ore, which means that the volume of fines (X_{mf}) should be less than the volume of solids (X_{ms}). According to Table 4.7, the volumetric flow-rate of rocks at the mill inlet (V_{mri}) is less than the volumetric flow-rate of solids at the mill inlet (V_{msi}). Thus, it is assumed that the volume of rocks (X_{mr}) in the mill is less than the volume

[1] Optimisation Toolbox^{TM} is a registered trademark of The MathWorks, Inc.

of solids (X_{ms}). Insufficient survey data is available to choose narrow ranges for the volumetric flow driving force (V_V) and the abrasion rate for rocks (ϕ_r). Therefore, the following constraints were chosen:

$$\begin{aligned} 3 < X_{mw} < 6,\ \ 3 < X_{ms} < 6,\ \ 0 < X_{mr} < 3 \\ 0 < X_{mf} < 3,\ \ 50 < V_V < 150,\ \ 1 < \phi_r < 50 \end{aligned} \tag{4.48}$$

The result of the minimization of eq. (4.47) is $X_{mw} = 4.85$ m^3, $X_{ms} = 4.90$ m^3, $X_{mf} = 1.09$ m^3, $X_{mr} = 1.82$ m^3, $\phi_r = 6.03$ kWh/t and $V_V = 84.0$.

4.3.2.3 Sump

The three states within the sump can be determined from eq. (4.28)-(4.30) since the volume of slurry in the sump ($SVOL$), the cyclone feed flow-rate (CFF) and the flow-rates out of the sump (V_{swo}, V_{sso} and V_{sfo}) are all available from survey data. Thus:

$$X_{sw} = \frac{V_{swo} SVOL}{CFF} = 4.11 \text{ m}^3 \tag{4.49}$$

$$X_{ss} = \frac{V_{sso} SVOL}{CFF} = 1.88 \text{ m}^3 \tag{4.50}$$

$$X_{sf} = \frac{V_{sfo} SVOL}{CFF} = 0.42 \text{ m}^3 \tag{4.51}$$

4.3.2.4 Hydrocyclone

There are six parameters to determine for the hydrocyclone module (C_1, C_2, C_3, C_4, ε_c, α_{su}). These parameters are found in eqs. (4.37) and (4.38). Two equations and six unknowns leave four degrees of freedom. From the description of the hydrocyclone model in Section 4.2.4, C_1 is equal to 0.6 and C_2 is equal to 0.7. Hulbert (2005) indicated that equal integer values for C_3 and C_4 are practical. For the flow-rate data of the cyclone in Table 4.7, the smallest integer value that results in a positive value inside the natural logarithm in eq. (4.52) is $C_3 = C_4 = 4$. The calculation of the parameter related to coarse split (ε_c) and the parameter related to fraction solids in the underflow (α_{su}) is shown below:

$$\varepsilon_c = \frac{-V_{cti}}{\ln\left(\frac{1}{C_1} - \frac{V_{ccu}}{V_{cci} C_1 \left(1 - \left(\frac{F_i}{C_2}\right)^{C_3}\right)\left(1 - P_i^{C_4}\right)}\right)} = 129 \tag{4.52}$$

$$\alpha_{su} = \frac{-V_{ccu}}{\varepsilon_c \ln\left(\frac{F_u - 0.6}{F_i - 0.6}\right)} = 0.87 \tag{4.53}$$

4.4 MODEL VALIDATION

A simulation platform was created in MATLAB and Simulink[2] to simulate the single-stage grinding mill circuit as described by the *Hulbert*-model. The platform was simulated for all five operating conditions of the sampling campaigns where the operating conditions are the five set-points for the grinding mill circuits.

In order to keep the sump from running dry or overflowing, a proportional-integral controller was used to keep the sump level at 1.0 m above the pump inlet by manipulating the cyclone feed flow-rate:

$$CFF = CFF_0 + K\left(e_l + \frac{1}{\tau}\int e_l dt\right) \tag{4.54}$$

where CFF_0 is the cyclone feed flow-rate of the third survey, $K = 20$ is the proportional gain, $\tau = 0.25$ is the integral reset and e_l is the error between the actual and desired sump level above the pump inlet.

4.4.1 Simulation

The manipulated variables in the simulation are the feed-rate of ore (MFS), water (MIW) and balls (MFB) to the mill, and the flow-rate of water to the sump (SFW), as described in Table 4.1. The simulation steps for these variables are shown in Fig. 4.5. The sequence of the input steps are as follows: Survey 3, Survey 4, Survey 5, Survey 1, Survey 2. The set of input variables that represent the operating condition of a survey are kept constant for 10 hours. Therefore, for the first 10 hours the model simulates the operating point of the third survey to which it was fitted. If a good fit was obtained, the output of the model should be similar to the actual steady-state outputs measured during the survey. When changing from one set-point to another, the input variables are ramped over a 10-hour period to reduce any excessive dynamic response in the output variables. The 10-hour period in which the manipulated variables are kept constant allows adequate time for the grinding mill to achieve a new steady-state and for any dynamic responses to have settled. It is in these 10-hour periods that the output variables of the simulation model can be compared with the actual steady-state sampling campaign data.

The *Hulbert*-model was simulated for two different cases. In the first, the power needed per tonne of fines produced (ϕ_f) was kept constant for all set-points at the value measured during the third survey.

[2]MATLAB and Simulink are registered trademarks of The MathWorks Inc.

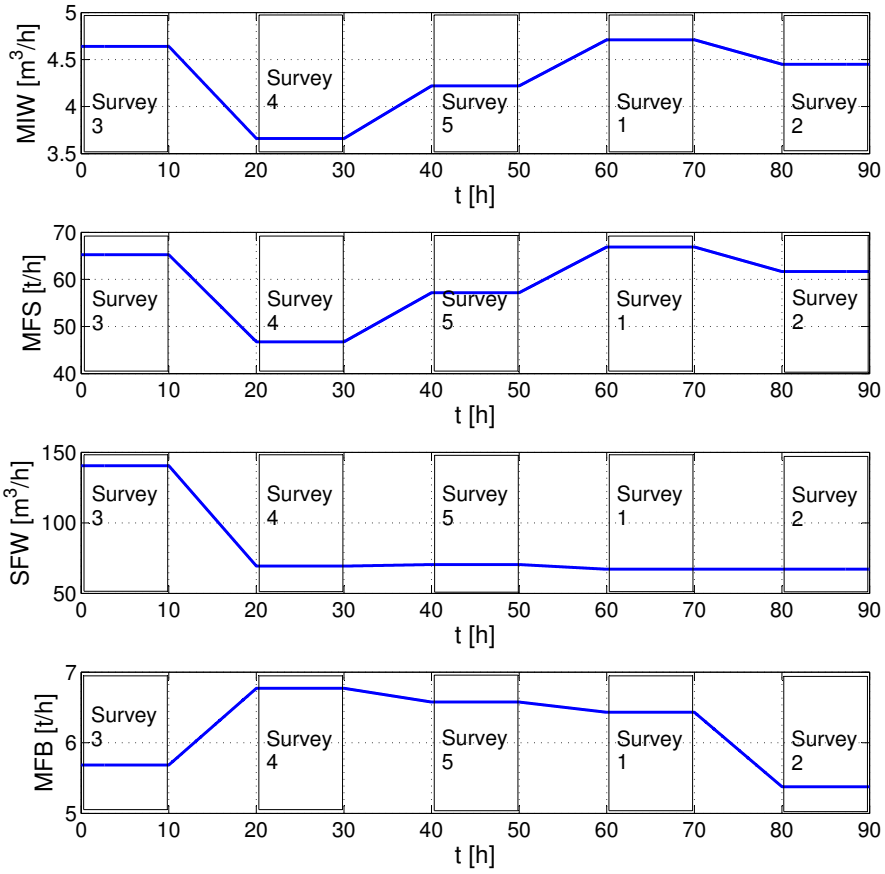

Figure 4.5: Inputs to grinding mill circuit.

In the second case, the power needed per tonne of fines produced (ϕ_f) was updated at the start of each new set-point according to survey data shown in Table 4.4, i.e. ϕ_f is an additional input with set-point values as shown in Table 4.4.

4.4.2 Results and Discussion

The output variables that are of interest in the model validation procedure are the product particle size (PSE), the volume of slurry in the sump ($SVOL$), the cyclone feed flow (CFF), the mill power draw (P_{mill}) and the fraction of the mill filled. However, only PSE, CFF and P_{mill} can be compared to actual survey data. The other two variables were not measured during the surveys.

The simulation output of the volume of slurry in the sump ($SVOL$) and the fraction of mill filled are shown in Fig. 4.6. The controller action is clearly visible in the $SVOL$. The significant change in $SVOL$ and fraction of milled filled between hours 10 and 20 is a result of the large reduction in the

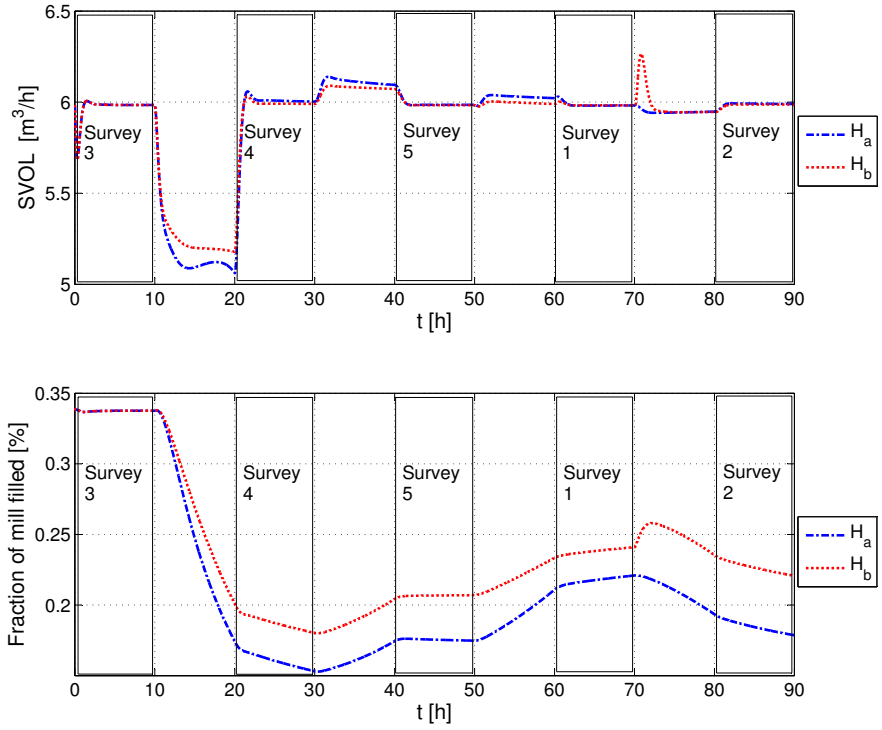

Figure 4.6: Sump volume ($SVOL$) and fraction of mill filled (JT). (H_a: *Hulbert*-model with constant ϕ_f, H_b: *Hulbert*-model with updated ϕ_f.)

flow-rate of water to the sump (SFW) between surveys 3 and 4.

The mill power draw (P_{mill}) is shown in Fig. 4.7. The steady-state values measured during each survey are shown by the solid line. Figure 4.7 shows that the mill power draw was fitted accurately to survey 3, since P_{mill} given by eq. (4.13) and the measured mill power draw for the third survey are the same. The trend that P_{mill} follows over the period of the simulation is similar to the trend followed by the fraction of the mill filled in Fig. 4.6. The *Hulbert*-model seems to change in the right direction with and without the power needed per tonne of fines produced (ϕ_f) being updated. In the case where ϕ_f is updated, the model is able to give a fair estimate of the actual mill power for surveys 1, 2 and 5.

The cyclone feed flow-rate (CFF) is shown in Fig. 4.8. The steady-state values measured during each survey are shown by the solid lines. Figure 4.8 shows that CFF as given by the *Hulbert*-model was fitted accurately to survey 3, since CFF given by eq. (4.54) and the measured cyclone feed flow for the third survey are almost equal. However, the model could not accurately estimate CFF for the other surveys, apart from survey 2. Differences between the controller used by the actual plant and

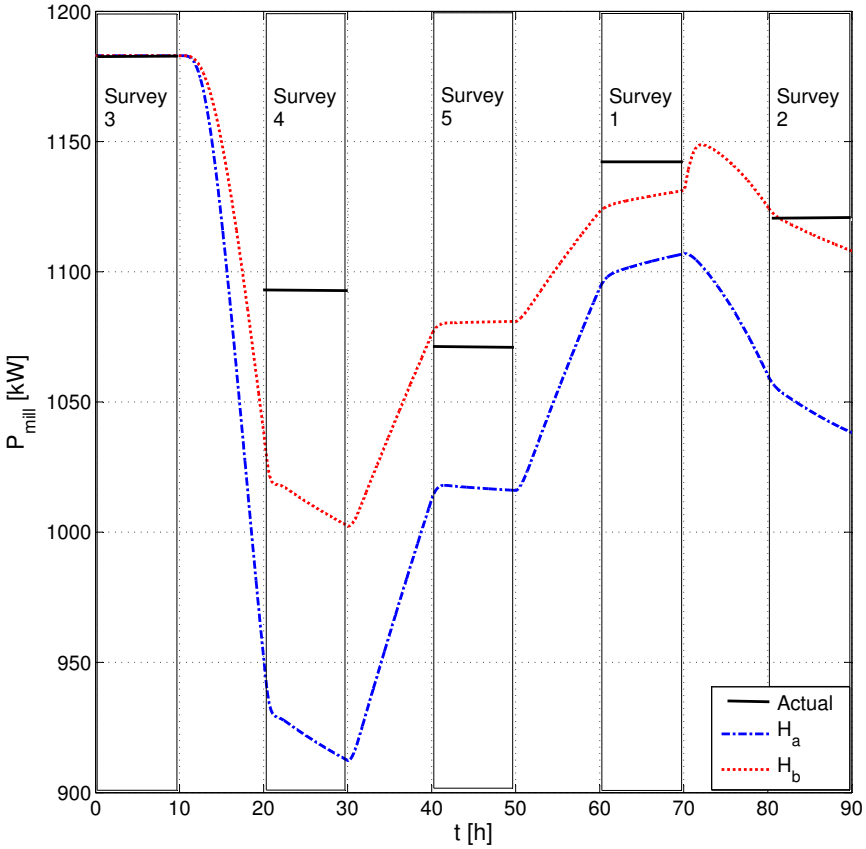

Figure 4.7: Mill power draw (P_{mill}). (Actual: sampling campaign data value, H_a: *Hulbert*-model with constant ϕ_f, H_b: *Hulbert*-model with updated ϕ_f.)

the controller used during simulation should not make a major difference on CFF in Fig. 4.8. At steady-state operation, the controller should no longer have any influence on CFF.

There are a few possible reasons for the poor estimation of CFF by the *Hulbert*-model for surveys 1, 4 and 5. The value of CFF is determined primarily by the flow-rate of water to the sump (SFW) plus how fast the mill discharges slurry. The latter is dependent on two factors in the mill: the viscosity (more water means higher flow) and the charge hold-up (higher volume means higher flow). These in turn are dependent on the flow-rate and content of water in the cyclone underflow (V_{cwu}). Because the cyclone underflow ties back to CFF, the main critical factor is the water content of the underflow. The higher CFF, the higher the water inflow, but the lower the water content of the underflow. However, the ratio of fresh feed of solids and water to the mill can be higher or lower than the ratio of the recycle, which means the cumulative effect could be a positive or negative gain, or both in different regions.

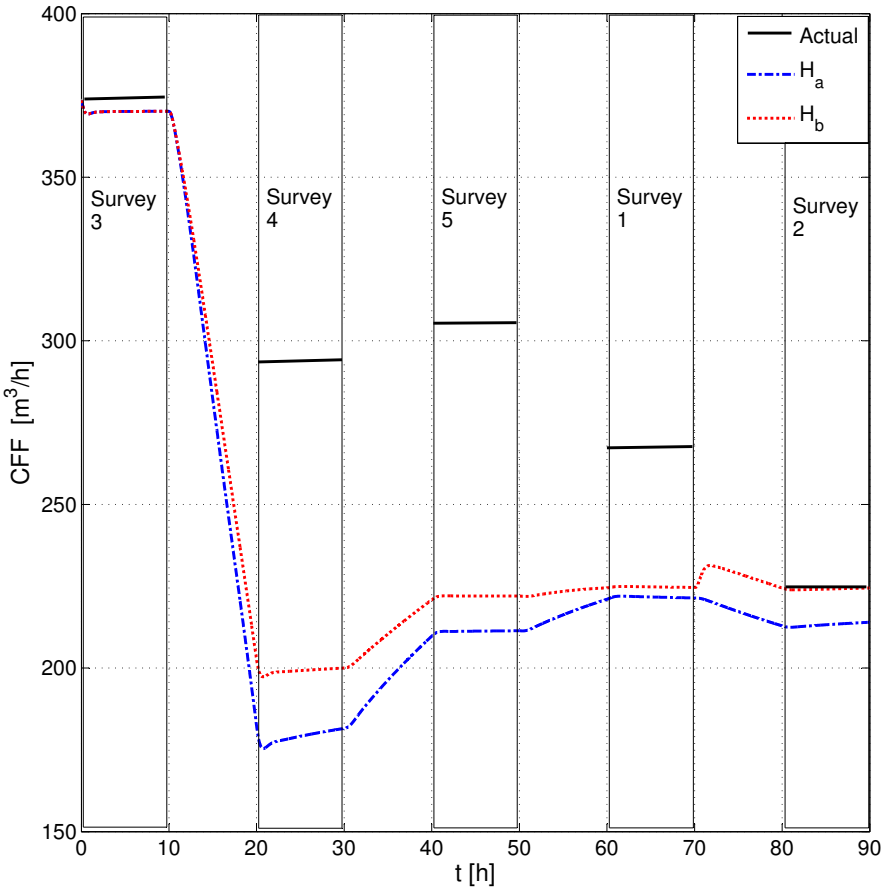

Figure 4.8: Cyclone feed flow (CFF). (Actual: sampling campaign data value, H_a: *Hulbert*-model with constant ϕ_f, H_b: *Hulbert*-model with updated ϕ_f.)

The product particle size estimate (PSE) shown in Fig. 4.9 indicates the percentage of ore that passes 75 μm for each survey. The steady-state values measured during each survey are shown by the solid lines. This figure shows that the PSE as given by the *Hulbert*-model was fitted accurately to the data of the third survey. For the other surveys (except survey 4), the *Hulbert*-model gives a fair estimate of the actual percentage of ore that passes 75 μm when the power needed per tonne of fines produced (ϕ_f) is updated at the start of each new set-point. The accurate estimation of PSE for surveys 1, 2 and 5 when ϕ_f is updated is a good result since all the other model parameters remain fitted to the data of survey 3. In the case of a constant ϕ_f for all the surveys, the *Hulbert*-model struggles to follow the same trend as the measured PSE. Because the product particle size can be measured on-line in grinding mill circuits, it should be possible to calculate ϕ_f and update this parameter whenever the operating condition of the plant is altered.

The PSE should not be influenced extensively by the value of CFF. The cyclone splits off the

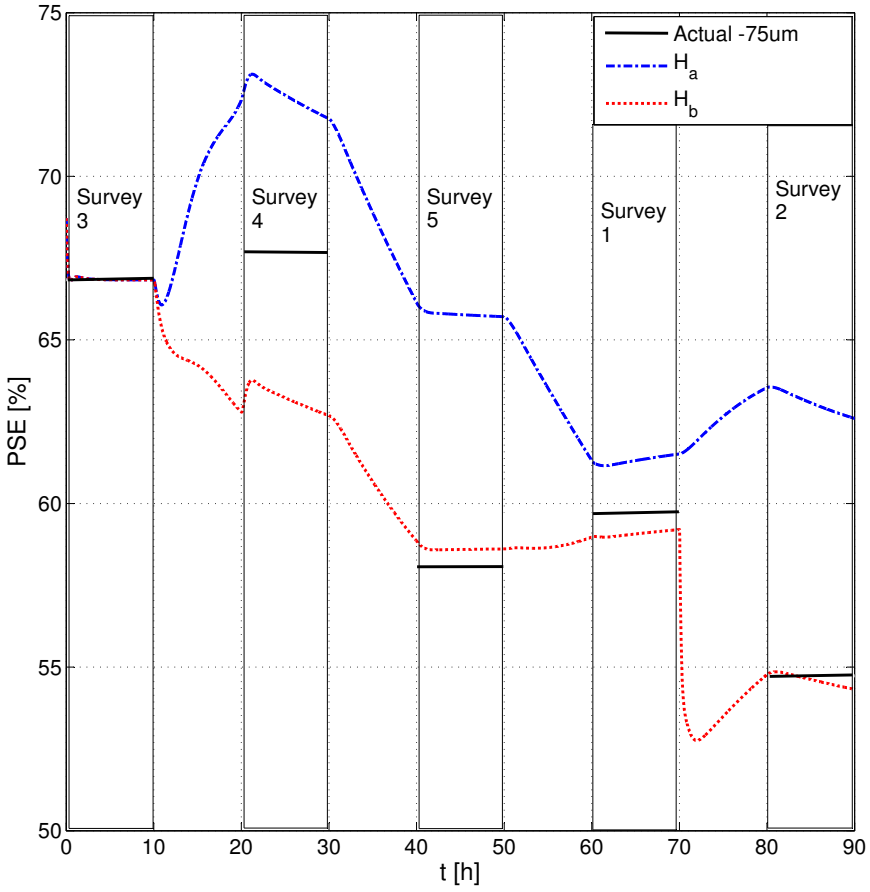

Figure 4.9: Particle size estimate (*PSE*). (Actual -75 μm: sampling campaign data value for ore passing 75 μm, H_a: *Hulbert*-model with constant ϕ_f, H_b: *Hulbert*-model with updated ϕ_f.)

coarse material back to the mill and makes the mill grind slightly differently. A high CFF tends to give particles a quicker interval between classification opportunities in the cyclone, reducing the fine material in the mill, making space for more coarse material to be ground and sharpening the slope of the size distribution of ore in the mill. The conditions in the mill are an integrated effect of the differences between inflows and outflows plus the effect of power and charge changes in the mill. The optimum fines production is determined by a sensitive balance of the conditions in the mill. Because grinding mill circuit operation normally chases the optimum condition, the gains of cause-and-effect are not large and linear near the optimum operating condition. Instead, the gains are relatively small and of either sign near the optimum. Therefore it is not surprising if *PSE* results at steady state are not predicted well when the power needed per tonne of fines produced (ϕ_f) is kept constant.

4.5 CONCLUSION

From Figs. 4.7-4.9 it is clear that the *Hulbert*-model was fitted satisfactorily to the data of the third survey. As the operating point is changed, the output variables of the model - except the cyclone feed flow (CFF) - change in the correct directions with orders of magnitude similar to the changes in survey data. The *Hulbert*-model gives a qualitatively accurate description of the mill power draw (P_{mill}) for a constant and an updated power needed per tonne of fines produced (ϕ_f) and for product particle size estimate (PSE) for an updated power needed per tonne of fines produced (ϕ_f). Although the results are promising, more data sets are required to fully verify the capabilities of the Hulbert-model.

A general procedure to fit the *Hulbert*-model to a single-stage grinding mill circuit was described in this chapter. The aim of the *Hulbert*-model is not to provide a tool for designing new grinding mill circuits. Rather, the model can be fitted to survey data with relative ease to provide a model that can be used to develop a control strategy for a grinding mill circuit. If one assumes full-state feedback, the model can be used in a control strategy such as the robust non-linear model predictive controller in Coetzee et al. (2010). Otherwise, the model can be used as a state-estimator if the input and output variables of the plant are available.

CHAPTER 5

CONCLUSION

This dissertation considers two non-linear dynamic models of a single-stage closed grinding mill circuit for process controller design. The main objective of the models are to ease process controller design in order to maintain the grinding mill circuit at optimal operation.

In the first part of the study, the number of size classes in a cumulative rates model of a grinding mill circuit was reduced to determine the minimum number required to provide a reasonably accurate model of the circuit for process control.

The second part of the study validated a simple and novel non-linear model of a run-of-mine ore grinding mill circuit developed for process control and estimation purposes. This model is named the *Hulbert*-model and makes use of the minimum number of states and parameters necessary to produce responses that are qualitatively accurate.

5.1 SUMMARY AND EVALUATION

5.1.1 Size class set reduction for a cumulative rates model

The cumulative rates model assumes that a single function, the cumulative breakage rate function (K_i^E), is sufficient to describe the grinding kinetics inside a mill. A reference size class set of 25 sizes separated by $\sqrt{2}$ was used to represent the ore in single-stage closed grinding mill circuit. This reference set was reduced to sets of 9, 5 and 3 log-linearly distributed sizes, and to sets of 9, 5 and 3 sizes with distributions that give the best straight-line approximation of K_i^E in the cumulative rates model. The non-linear cumulative rates models defined by the reference size class set and the other six new sets were linearized by means of system identification in order to design seven linear model

predictive controllers. The linear controllers were implemented on a grinding mill circuit simulated by the non-linear cumulative rates model based on the reference set of 25 size classes. The performance of the controllers based on the reduced size class sets were compared to the performance of the controller based on the reference size class set. The similarity between controller performance was used as an indication of the accuracy with which a reduced size class set modelled the circuit.

Nine size classes, irrespective of the size class distribution, and 5 size classes defined to best represent K_i^E, produced model predictive controllers that gave almost identical results to the model predictive controller based on 25 size classes. This was expected since the model parameters of the linear transfer functions for these four size class sets were almost the same. The model with 3 size classes defined to best represent K_i^E is as accurate as the model with 5 log-linearly distributed size classes. The latter two size class sets model the circuit with similar rates and magnitudes of changes as the model with 25 sizes and can be regarded as fairly accurate. The model with 3 log-linearly distributed size classes could only indicate the directions of the changes in process variables, but the model predictive controller based on this size class set was able to control the circuit and maintain the product particle size (PSE) at setpoint.

A model with a large size class set provides valuable information for plant design and scale-up, whereas a model with a small size class set may be more suited for process control. In a non-linear MPC scheme, a reduced size class set lessens the number of differential equations to solve when predicting the future behaviour of the plant. This reduces the computational burden compared to a model in a non-linear MPC scheme that uses 25 size classes. However, the increase in computational power according to Moore's law will allow future processors to handle large size class set models in non-linear MPC schemes with ease.

To develop an accurate model for process control, a sampling campaign does not need to measure as many as 25 size classes. It is possible to evaluate 9 size classes in a sampling campaign, but only use a selection of 5 size classes to model the circuit. As seen from the linearized models, when K_i^E is represented by a reduced size class set the model of the grinding mill circuit remains almost as accurate as the model with the full size class set. With fewer size classes more degrees of freedom are available to fit the breakage rate function parameters. However, if only a few size classes are used more care should be taken to ensure the size class set distribution captures the non-linear behaviour of K_i^E. A poor representation of K_i^E will result in a deterioration of model accuracy. Although as few as 3 size classes can be used to obtain a fairly accurate model, the distribution of the 3 size classes

influences the accuracy of the model. For a model to be useful for process control, the model should at least provide the directions in which the process variables change.

5.1.2 Analysis and validation of a grinding mill model for process control

The simple non-linear *Hulbert* model was developed in view of the fact that it is possible to use only a few size classes to create a model that can be used to control a grinding mill circuit.

The *Hulbert*-model makes use of the minimum number of states and parameters necessary to produce responses that are qualitatively accurate. It consists of separate feeder, mill, sump and hydrocyclone modules that can be connected to model a variety of circuit configurations. The hydrocyclone module is novel. The model uses five states to present the material in the milling circuit: rocks, solids, fines, water and steel balls. Rocks are defined as too large to be discharged from the mill, whereas solids, defined as particles small enough to leave the mill, consist of out-of-specification coarse ore and in-specification fine ore fractions. The *Hulbert*-model incorporates a unique prediction of the rheology of the slurry within the mill.

A general procedure to fit the model to steady-state data was illustrated by fitting the model to sampling campaign data of an actual plant. As seen from the simulated results, the model was fitted satisfactorily. Since sampling campaign data was available for operating conditions of the plant other than the one used to fit the model, the fitted model was simulated for these operating conditions. The simulated results indicate that the *Hulbert*-model gives a qualitatively accurate description of the mill power draw (P_{mill}) for a constant and an updated power needed per tonne of fines produced (ϕ_f) and for product particle size estimate (PSE) for an updated power needed per tonne of fines produced (ϕ_f).

This study is part of an ongoing endeavour to show the abilities of the *Hulbert*-model to be used as a tool for generating a good process model at low cost, developing a practical high-fidelity observer and designing an effective control strategy for a grinding mill circuit. The *Hulbert*-model shows promise in estimating important process variables such as mill power and product particle size and is deemed suitable for process control studies.

5.2 RECOMMENDATIONS FOR FURTHER WORK

The cumulative rates model assumes that the cumulative rate of breakage of ore above size x_i is unaffected by the grinding environment and the structure of the size distribution of size x_i. A possible improvement for this model is to account for changes in grinding conditions by manipulating the cumulative breakage rate function.

Since the breakage of ore in the cumulative rates model is a function of the power drawn by the mill, the accuracy of the model may possibly improve with the use of a different power draw equation. The power draw predicted by the model of Austin (1990), which is used in this study, does not allow for large dynamic variations in mill power. The power draw model used by Morrell (2004) might be a more accurate prediction of the mill power draw.

The grindcurves developed by Powell et al. (2009) indicates that maximum circuit throughput does not necessarily correspond with maximum mill power draw. The ability of the cumulative rates model and the *Hulbert*-model to reproduce grindcurves may be additional validation of these models.

In the hydrocyclone module of the *Hulbert*-model, the assumption is made that the ratio of fines to water in the under-, over- and in-flow remains constant. This assumption is not always true and provides opportunity for further improvement of the model.

This study validated the *Hulbert*-model with data from a SAG mill with a fairly large ball load. A further indication of the accuracy of the model will be provided if the model is fitted to a SAG mill with a smaller ball load, an AG mill and a ball mill with a crushed ore feed. If dynamic plant data is available, an interesting comparison study can be made between dynamic data, the *Hulbert*-model dynamics and also the validated dynamic model in Apelt et al. (2002).

REFERENCES

Amestica, R., Gonzalez, G. D., Barria, J., Magne, L., Menacho, J., and Castro, O. A SAG mill circuit dynamic simulator based on a simplified mechanistic model. *XVIII International Mineral Processing Congress*, Sydney:117–129, 1993.

Amestica, R., Gonzalez, G. D., Menacho, J., and Barria, J. A mechanistic state equation model for semiautogenous mills. *Int. J. Mineral Process.*, 44-45(SPEC. ISS.):349 – 360, March 1996.

Apelt, T. A., Asprey, S. P., and Thornhill, N. F. Inferential measurement of SAG mill parameters. *Minerals Eng.*, 14(6):575–591, Feb. 2001.

Apelt, T. A., Asprey, S. P., and Thornhill, N. F. Inferential measurement of SAG mill parameters II: State estimation. *Minerals Eng.*, 15(12):1043–1053, Sept. 2002.

Apelt, T. and Thornhill, N. Inferential measurement of SAG mill parameters IV: inferential model validation. *Minerals Eng.*, 22(12):1032–1044, 2009.

Austin, L. G. A mill power equation for SAG mills. *Minerals Metallurgical Process.*, 7(1):57–63, 1990.

Austin, L. G. and Klimpel, R. R. The back-calculation of specific rates of breakage from continuous mill data. *Powder Technol.*, 38(1):77–91, 1984.

Austin, L. G., Sutherland, D. N., and Gottlieb, P. An analysis of SAG mill grinding and liberation tests. *Minerals Eng.*, 6(5):491–507, 1993.

Bascur, O. A. and Herbst, J. A. Dynamic simulator for training personnel in the control of grinding and flotation systems. In *Proc. 5th IFAC Symposium Mining Metallurgy*, Brisbane, Australia, 1985.

Bauer, M. and Craig, I. K. Economic assessment of advanced process control - A survey and framework. *J. Process Control*, 18(1):2–18, Jan. 2008.

Chen, X., Zhai, J., Li, S., and Li, Q. Application of model predictive control in ball mill grinding circuit. *Minerals Eng.*, 20(11):1099 – 1108, Sept. 2007.

Chen, X., Li, Q., and Fei, S. Constrained model predictive control in ball mill grinding process. *Powder Technol.*, 186(1):31 – 39, Aug. 2008.

Chen, X., Yang, J., Li, S., and Li, Q. Disturbance observer based multi-variable control of ball mill grinding circuits. *J. Process Control*, 19(7):1205 – 1213, 2009.

Coetzee, L. C. *Robust Nonlinear Model Predictive Control of closed run-of-mine ore milling circuit*. PhD thesis, Unversity of Pretoria, June 2009.

Coetzee, L. C., Craig, I. K., and Kerrigan, E. C. Robust nonlinear model predictive control of a run-of-mine ore milling circuit. *IEEE Trans. Control Syst. Technol.*, 18(1):222–229, January 2010.

Craig, I., Aldrich, C., Braatz, R., Cuzzola, F., Domlan, E., Engell, S., Hahn, J., Havlena, V., Horch, A., Huang, B., Khanbaghi, M., Konstantellos, A., Marquardt, W., McAvoy, T., Parisini, T., Pistikopoulos, S., Samad, T., Skogestad, S., Thornhill, N., and Yu, J. The Impact of Control Technology: Control in the process industries, 2011. T. Samad and A.M. Annaswamy (Eds.), Available at www.ieeecss.org.

Craig, I. K. and MacLeod, I. M. Specification framework for robust control of a run-of-mine ore milling circuit. *Control Eng. Practice*, 3(5):621–630, May 1995.

Craig, I. and MacLeod, I. Robust controller design and implementation for a run-of-mine ore milling circuit. *Control Eng. Practice*, 4(1):1–12, Jan. 1996.

Dochain, D., Marquardt, W., Won, S., Malik, O., Kinnaert, M., and Lunze, J. Monitoring and control of process and power systems: Adapting to environmental challenges, increasing competitivity and changing customer and consumer demands. In *Proc. 17th IFAC World Congress*, Seoul, Korea, 6-11 July, 2008.

Gupta, A. and Yan, D. S. *Mineral processing design and operation: An introduction*. Elsevier B. V.,

2006.

Hinde, A. L. External Report (Confidential). Technical report, Mintek, 2009.

Hinde, A. L. and Kalala, J. T. The application of a simplified approach to modelling tumbling mills, stirred media mills and HPGR's. *Minerals Eng.*, 22(7-8):633–641, April 2009.

Hinde, A. L. and King, R. P. Difficulties in the practical implementation of mill control systems. In *Proc. 11th Commonwealth Mining Metallurgical Congress*, Hong Kong, May 1978.

Hodouin, D. Methods for automatic control, observation and optimization in mineral processing plants. *J. Process Control*, 21(2):211–225, Feb. 2011.

Hodouin, D., Jamsa-Jounela, S., Carvalho, M., and Bergh, L. State of the art and challenges in mineral processing control. *Control Eng. Practice*, 9(9):995 – 1005, Sept. 2001.

Hulbert, D. G. Simulation of milling circuits: Part 1 & 2. Technical report, Mintek, Johannesburg, South Africa, 2005.

Hulbert, D. Multivariable control and optimization of the operation of a milling circuit at east driefontein gold mine. Technical report, MINTEK, Report M98, 1983.

King, R. P. *Modeling and simulation of mineral processing systems*. Butterworth Heinemann, 2001.

Laplante, A., Finch, J., and del Villar, R. Simplification of grinding equation for plant simulation. *Trans. Inst. Mining Metallurgy, Sect. C: Mineral Process. Extractive Metallurgy*, 96:c108–c112, 1987.

le Roux, J. D. and Craig, I. K. Reducing the number of size classes in a cumulative rates model used for process control of a grinding mill circuit. *Powder Technol.*, 2012. Submitted for Review.

le Roux, J. D., Craig, I. K., Hulbert, D. G., and Hinde, A. L. Analysis and validation of a run-of-mine ore grinding mill circuit model for process control. *Minerals Eng.*, 2012. Articles in Press.

Mishra, B. A review of computer simulation of tumbling mills by the discrete element method: Part I - contact mechanics. *Int. J. Mineral Processing*, 71(1-4):73–93, 2003a.

Mishra, B. A review of computer simulation of tumbling mills by the discrete element method: Part II - practical applications. *Int. J. Mineral Processing*, 71(1-4):95–112, 2003b.

Morrell, S. A new autogenous and semi-autogenous mill model for scale-up, design and optimisation. *Minerals Eng.*, 17(3):437–445, March 2004.

Nageswararao, K., Wiseman, D. M., and Napier-Munn, T. J. Two empirical hydrocyclone models revisited. *Minerals Eng.*, 17(5):671–687, May 2004.

Napier-Munn, T. J., Morrell, S., Morrison, R. D., and Kojovic, T. *Mineral Communition Circuits: Their Operation and Optimisation*. JKMRC Monograph Series in Mining and Mineral Processing, 2nd edition, 1999.

Narasimha, M., Brennan, M., and Holtham, P. CFD modeling of hydrocyclones: Prediction of particle size segregation. *Minerals Eng.*, 39:173–183, 2012.

Pomerleau, A., Hodouin, D., Desbiens, A., and Gagnon, E. A survey of grinding circuit control methods: from decentralized PID controllers to multivariable predictive controllers. *Powder Tech.*, 108(2-3):103 – 115, 2000.

Powell, M. S. and Morrison, R. D. The future of comminution modelling. *Int. J. Mineral Process.*, 84(1-4):228–239, Oct. 2007.

Powell, M., van der Westhuizen, A., and Mainza, A. Applying grindcurves to mill operation and optimisation. *Minerals Eng.*, 22(7-8):625–632, June 2009.

Powell, M., Perkins, T., and Mainza, A. Grindcurves applied to a range of SAG and AG mills. In *Proc. SAG 2011*, Vancouver, B.C., Canada, 2011.

Qin, S. J. and Badgwell, T. A. A survey of industrial model predictive control technology. *Control Eng. Practice*, 11(7):733–764, 2003.

Ramasamy, M., Narayanan, S. S., and Rao, C. D. P. Control of ball mill grinding circuit using model predictive control scheme. *J. Process Control*, 15(3):273–283, 2005.

Salazar, J. L., Magne, L., Acuña, G., and Cubillos, F. Dynamic modelling and simulation of semi-autogenous mills. *Minerals Eng.*, 22(1):70 – 77, 2009.

Shi, F. N. and Napier-Munn, T. J. Effects of slurry rheology on industrial grinding performance. *Int. J. Mineral Process.*, 65(3-4):125–140, July 2002.

Soderstrom, T. and Stoica, P. *System Identification*. Prentice Hall International, University Press, Cambridge, 1989.

Song, C., Wang, P., and Makse, H. A. A phase diagram for jammed matter. *Nature*, 453(7195): 629–632, May 2008.

Stanley, G. G. *The extractive metallurgy of gold in South Africa*, volume 1. South African Institute of Mining and Metallurgy, Johannesburg, 1987.

Steyn, C. Optimisation of a fully autogenous comminution circuit. Master's thesis, University of Pretoria, December 2011.

Valery Jr., W. and Morrell, S. The development of a dynamic model for autogenous and semi-autogenous grinding. *Minerals Engineering*, 8(11):1285–1297, 1995.

Viklund, T., Albertsson, J., Burstedt, J., Isaksson, M., and Soderlund, J. Evolution of AG mill control system at Boliden Mineral AB. In *Proc. SAG 2006*, Vancouver, B.C., Canada, 2006.

Wei, D. and Craig, I. K. Economic performance assessment of two ROM ore milling circuit controllers. *Minerals Eng.*, 22(9-10):826–839, Aug. 2009a.

Wei, D. and Craig, I. K. Grinding mill circuits - A survey of control and economic concerns. *Int. J. Mineral Process.*, 90(1-4):56 – 66, Feb. 2009b.

Whiten, W. J. A matrix theory of communition machines. *Chemical Eng. Sci.*, 29(2):589–599, 1974.

Wills, B. A. *Wills' mineral processing technology: an introduction to the practical aspects of ore treatment and mineral recovery*. Butterworth Heinemann, 7th edition, 2006.

“Men love to wonder, and that is the seed of science.”

- Ralph Waldo Emerson